University of Nairobi

College of Architecture and Engineering

Institute of Nuclear Science and Technology

Design, Fabrication and Optimization of a Water-vapor Condenser

by

Kiriinya Lindah K.

S56/71526/2014

BSc. Environmental and Bio-systems Engineering

A thesis submitted in partial fulfillment for the degree of Master of Science in Nuclear Science at the Institute of Nuclear Science and Technology in the University of Nairobi.

Declaration

This thesis is my original idea and has not been presented for a research in this or any other university.

Miss. Kiriinya Lindah Karea
S56/71526/2014

Sign ……..…..... Date: …….....……

Supervisors' approval

This thesis has been submitted with our knowledge as university supervisors.

Prof. Michael J. Gatari
Institute of Nuclear Science and Technology
University of Nairobi, Kenya

Sign ……..……..
Date: ……

Prof. Jan C. M. Marijnissen
Universities of Florida, USA and
Nairobi, Kenya

Sign …….
Date: ……

Dr. Luewton Lemos Agostinho
NHL, University of Applied Sciences
Leeuwarden, Netherlands

Sign ……..
Date: …….

Acknowledgement

I would like to thank God for keeping me in good health during the course of my study. I will forever be grateful to my mum, dad, brother and sister (The Kiriinya Family) and my son Baraka for their continued love and support during my studies.

My heartfelt gratitude to my supervisor's, Prof. Gatari and Prof. Jan Marijnissen. Their believe in my academic abilities and their guidance gave me strength when the going got tough. Prof Luewton Agostinho for hosting, guiding and supervision while in his laboratory using modeling facilities. The International Science Programme at Uppsala University, Sweden is appreciated for supporting my research in Kenya and the Netherlands.

My colleagues at the INST, UoN are warmly appreciated; Fredrick Kariithi for taking the time to go through my thesis; Susan Karuga for your useful input; Nahashon Nyambane for the interesting discussions; Mathias Mailu, Peter Ndwiga, Mary Karuiru and others

CONTENTS

List of Figures

List of Tables

Abstract

A thermal desalination system that relies on solar energy for water evaporation is currently under development at the Institute of Nuclear Science and Technology (INST), University of Nairobi. The system uses the electrospray technique to break up the water into small droplets. This creates a large surface area for evaporation. Such a system is comprised of evaporation and condensation processes. This study reports on the Design, Fabrication and Optimization of a Water-vapor Condenser from the evaporation process. To study the condensation process, an evaporation chamber was constructed and the physical and flow properties of the moist air [relative humidity, temperature, mass flow rate, velocity] were used as the input parameters for the condensation process. The condenser was then modeled using the iterative process provided in Kern method (1950). Using the results from the model, an experimental condenser was fabricated and measurements were carried out to investigate its performance. From experiments, the condenser efficiency was 41% for a relative humidity of 70% and condenser inlet water temperature of 20 ^{o}C; and 54% for a relative humidity of 70% and condenser inlet water temperature of 5 ^{o}C. It was observed that higher relative humidity favors condensation and a relative humidity lower than 40% produces very little condensation. The results from the experiment and the simulation showed on average a 15% deviation; thereby the simulation results could be relied upon to give an indication of the performance of the condenser. The highest simulated efficiency the system achieved was 78% which is comparable to the existing condensers that have efficiency range of 80 -85%. The average rise in temperature ΔT of the cooling water was 2^{o}C. It was also observed that the larger the temperature difference (ΔT) between the warm and cold fluid streams of the condenser the higher the rate of condensation.

Chapter One

Introduction

1.1 Background

Water is a necessity of life. Human beings, like any other living thing, require water for survival. The UN (2010), OHCHR (2010) and UN-HABITAT (2010) recommends that an average human being requires 50 liters of water for drinking, cooking and proper sanitation. Seventy percent (70%) of the earth's surface is covered by water. However, about 97.5% of water on the earth's surface is salty while 2.5% is fresh water with 80 % of this amount frozen in ice caps leaving only 0.5% for human and industrial use, (Mishra and Dubey, 2015). The fast rise in population and economic growth particularly in developing countries where safe water supply and proper sanitation remains a major challenge, continue to put pressure on the available water resources.

WHO (2006) and UNICEF (2006) observed that only 16% of the African population have access to drinking water through domestic connection. A domestic connection in this context is defined as an indoor tap or a tap in the yard. The situation in rural Africa is even worse due to poor infrastructural development. The water sources in these regions are mainly ground and surface water. However, the surface water sources are often highly polluted posing a serious health hazard. The underground water is also highly exploited causing receding ground water levels (Taylor *et al*., 2006). This contributes to increased salinity especially in Arid and Semi-Arid Lands (ASALs) where many cases of abandoned boreholes are reported. The inadequate access to water results in people having to travel long distances in search of water. Fetching water is mainly a role of women and young girls. This negatively impacts their livelihood and development since their capacity to engage in meaningful economic activities and attending school is unacceptably compromised.

Various policies and strategies have been put forward by governments and organizations to address this problem. Sea and borehole water desalination has been proposed as one of the suitable techniques that may be utilized to increase availability of clean water. The process involves separating dissolved salts and other minerals from water. Desalination is achieved through thermal or membrane processes.

One of the major drawbacks of this process is the high energy costs. However, incorporating cheap renewable energy options, like solar energy, will drive down the energy costs making desalination more economical. Therefore, regions characterized with long hours of solar energy

supply, like Africa, can harness this energy to run thermal desalination processes. The process is a technique that uses energy to evaporate water and then condense the water vapor. This process converts the influent into two streams: a fresh water stream and a high salt concentration stream (brine). For the thermal system to work efficiently, both the evaporation and the condensation processes should be optimized. This study focused on the design, fabrication and optimization of a condensation system for an innovated electrospray desalination system. The work involved design and fabrication of a water vapor condenser and investigation to find out its performance.

1.2 Statement of the Problem

Fresh water resources in the world are limited and are continually facing pressure from increasing domestic and commercial consumption. According to records held by WHO (2006), UNICEF (2006) and WWI (2006), it is estimated that 2.4 billion people have inadequate sanitation and another 1.1 billion are grappling with inadequate access to safe water. Water scarcity and stress pose a huge health risk especially in developing countries. It affects 1 in 3 people in the African Region and the situation is becoming more alarming with population increase, urbanization and increasing domestic and commercial uses (WHO, 2012). WWI (2006) and WHO (2006) reported that 1.6 million people die annually due to poor sanitation and unsafe drinking water. Kenya being a water stressed country with about 30% of its citizenry living in Arid and Semi-arid Lands (FAO, 2015) needs to explore innovative methods of ensuring adequate supply of clean and safe drinking water. It is imperative, therefore, that non-conventional techniques such as water desalination are considered to address not only the problem of water supply and quantity, but also water quality.

1.3 Justification

A noted rise in population over the last century and increasing commercial uses are stressing the existing fresh water resources. Different techniques are being explored to increase fresh water supply. Desalination presents a unique approach to address the fresh water scarcity due to its ability to make unusable water resources such as; sea-water, brackish water, highly saline ground water, polluted surface water; available as fresh water.

In Kenya, for example, 80% of her land area is classified as ASALs and about 10 million of her citizenry live here, representing 30% of the Kenyan population (FAO, 2015). In the ASALs, the available water is ground water but it is characterized by very high levels of salinity making it unfit for human consumption.

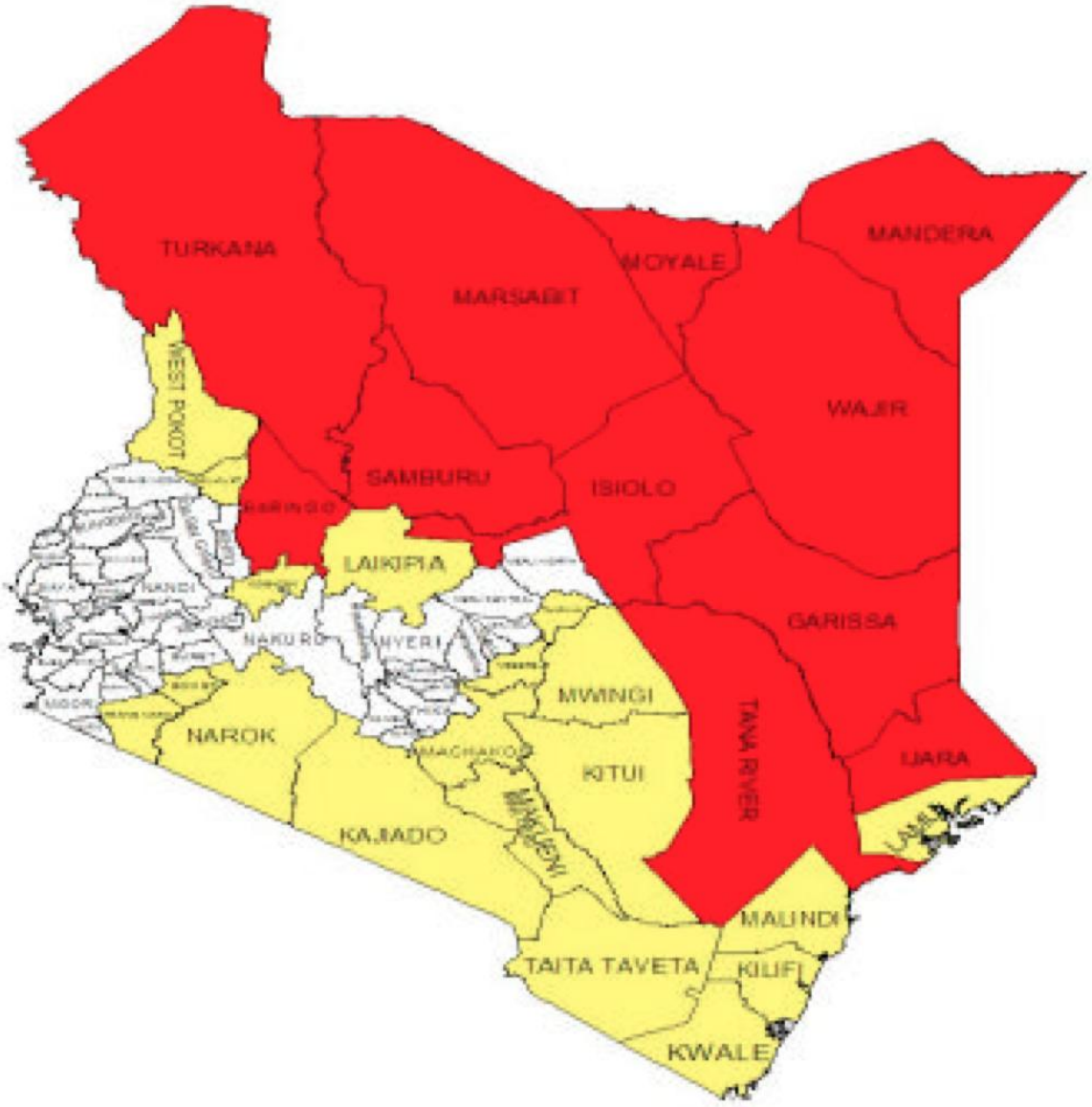

Figure 1. Map of arid and semiarid lands in Kenya shown in red and yellow respectively (Adopted from FA0, 2015).

Jingwe *et al* (2011) have shown that an evaporation based thermal desalination system can produce recovery ratio as high as 90%. Due to its high energy consumption, sustainable renewable energy technologies like solar can be incorporated thus making desalination a viable option for tropical countries that have long hours of sunlight. This was the basis of the development of an innovative electrospray desalination system at the Institute of Nuclear Science and Technology, University of Nairobi, but it needed an efficient water vapor condensing system which is therefore the focus of this study.

1.4 Scope of the Study

The experiments were carried out using an evaporation chamber to determine the moist air properties such as relative humidity, temperature and the evaporation efficiency at specified mass flow rate of water in the desalination system. Modeling was involved in designing and evaluating performance of the condenser. The condenser was then fabricated and further experiments carried out to determine its performance. Validation of the model was carried out by comparing the experimental results with the model output.

1.5 Objectives

The overall objective of this study was to design and fabricate a water vapor condenser using moist air properties (relative humidity, temperature and) as the input parameters, and investigate its efficiency under different conditions so as to determine optimal operating conditions

Specific Objectives

- To carry out experiments to determine the relative humidity, temperature and mass flow rate of moist air properties of vapor from evaporator.
- To model a condenser based on the Kern Design Method
- To fabricate a condenser using locally available materials
- To carry out experiments to determine the efficiency of the condenser
- To run simulations using Matlab/Simulink program so as to predict condenser performance (efficiency) under different conditions of moist air relative humidity, mass flow rate and cooling water temperature.
- To validate analysis by comparing the simulated and experimental results

Chapter Two

Literature Review

2.1 Heat Exchangers

A condenser is a heat exchanger. Heat exchangers are generally equipment designed to allow for efficient transfer of heat energy between one or more fluids, or between a solid and a fluid. For the exchange of heat energy to take place, there must be a temperature gradient and thermal contact between the different media.

2.1.2 Classification of Heat Exchangers

Heat Exchangers are categorized based on the following criteria: regenerators or recuperators; flow arrangement; geometry of construction; heat transfer mechanisms and transfer processes, through direct or indirect contact (Kakaç *et.al*, 2012). Kakaç (2012), classified them based on flow arrangement, number of fluids, surface compactness, construction, transfer process and heat transfer mechanisms (Figure 2).

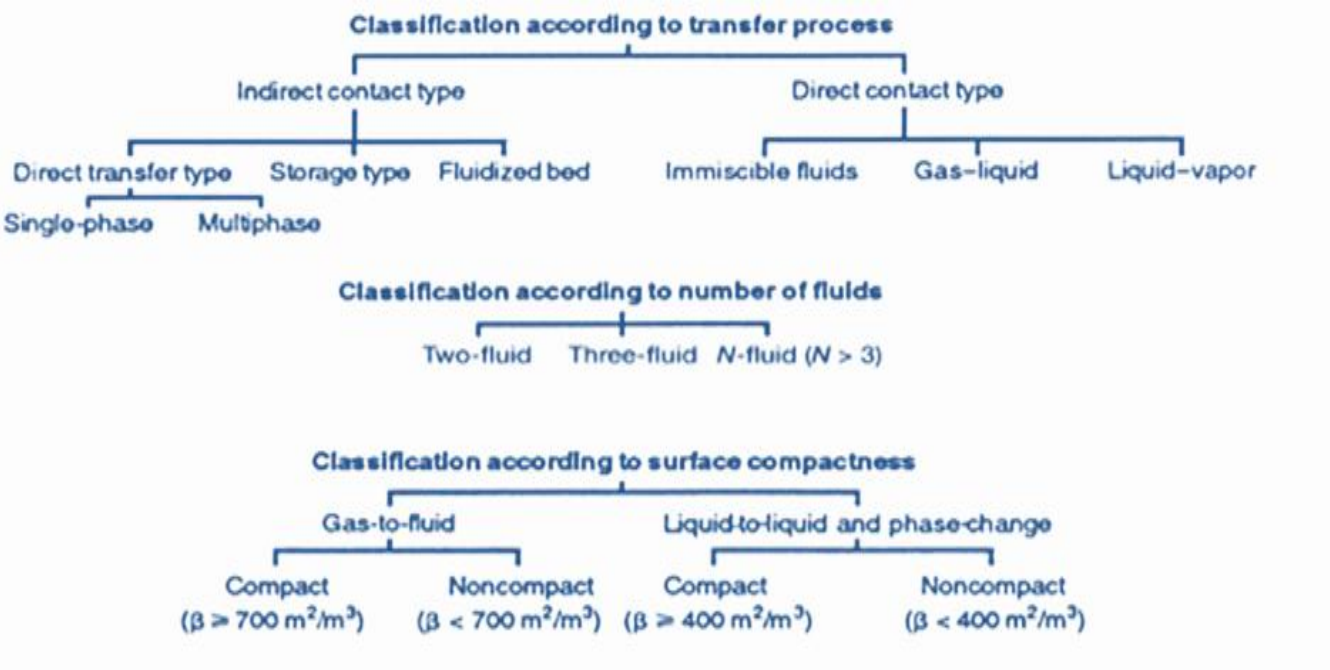

Figure 2a. Classification of Heat Exchangers (Adopted from Kakaç *et.al.*, 2012)

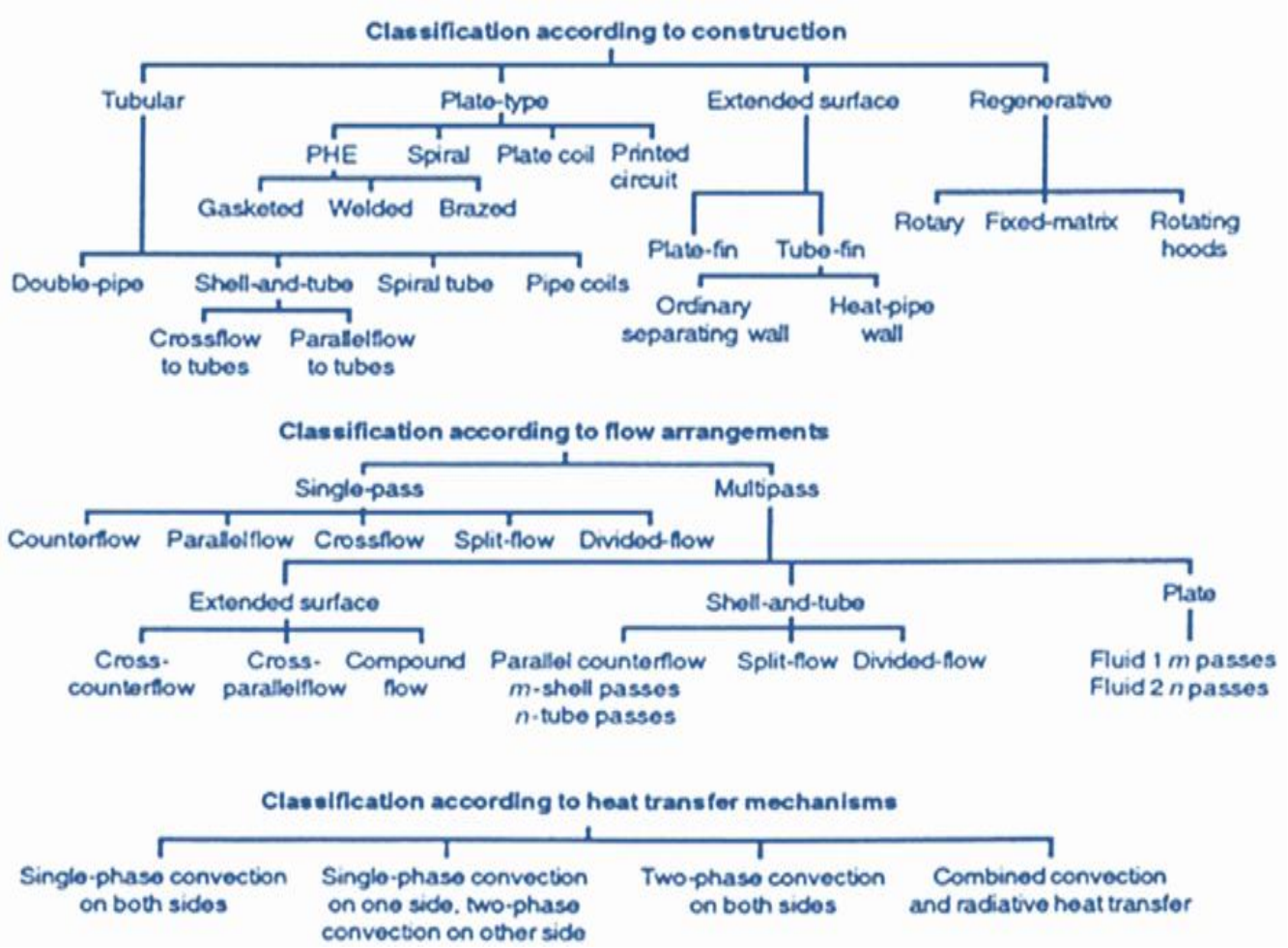

Figure 2b. Classification of Heat Exchangers (Adopted from Kakaç *et.al.*, 2012)

The Shell and Tube Heat Exchanger (STHE) (Figure 3) is the most widely used because of its relatively simple construction and its ability to adapt to different process requirements. According to Rajput (2008), the STHE are commonly classified according to their relative direction of fluid motion. In *parallel flow* STHE, the hot fluid and cold fluid streams move together in the same direction. The temperature gradient between the two fluids decreases as it flows from the inlet to the outlet. For this reason, the *parallel flow* STHE requires a large surface area for transfer of heat.

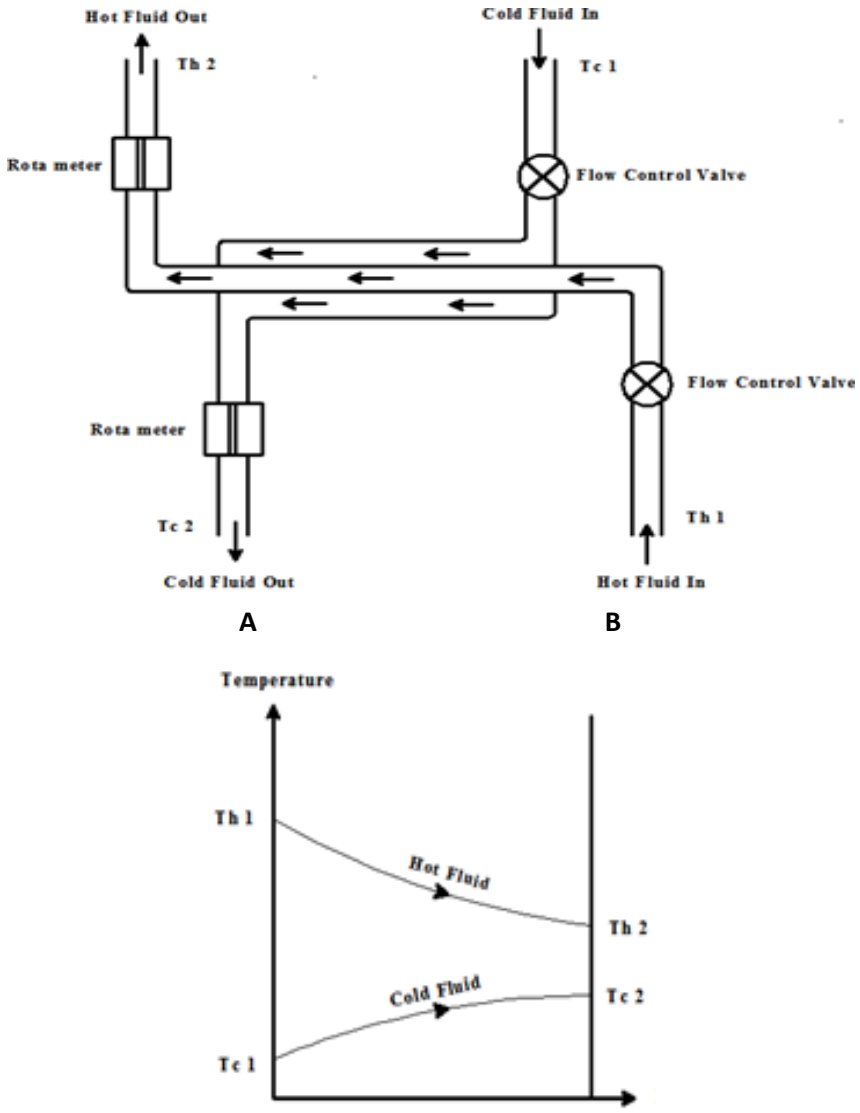

Figure 3. Flow arrangement and Temperature distribution in parallel flow STHE

(Adopted from Incopera *et.al.*, 2007)

The hot fluid stream and cold fluid stream move in opposite directions of each other in *counter flow* STHE. In this arrangement, as the hot and cold fluids flow from the inlet to the outlet, the temperature gradient remains constant (*See Figure 4*) resulting in a higher rate of heat transfer over a given surface area.

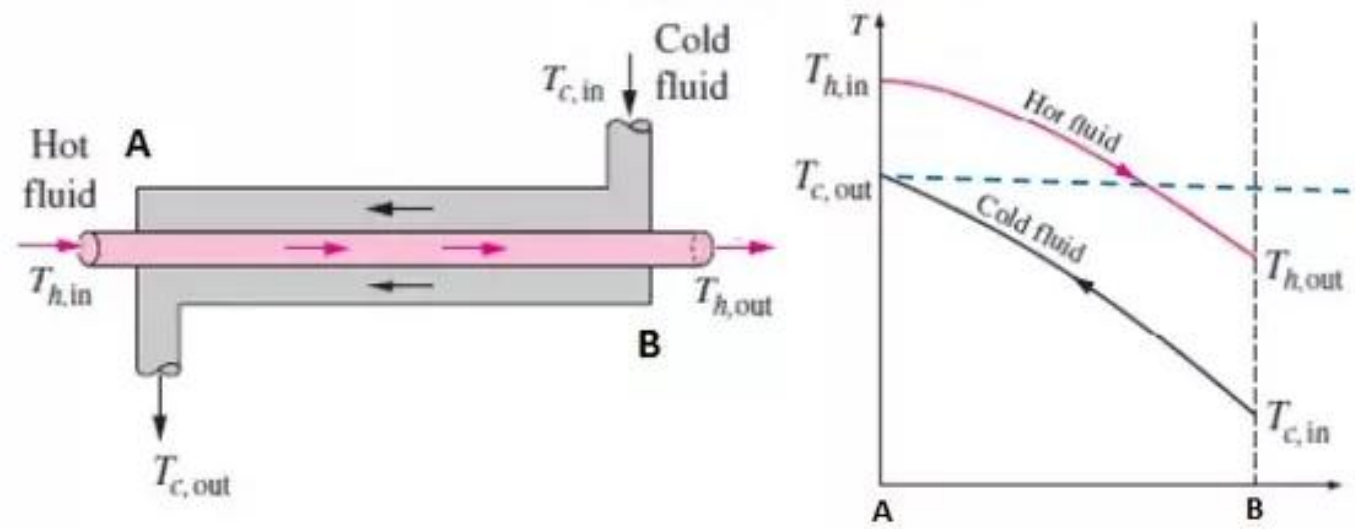

Figure 4. Flow arrangement and Temperature distribution in counter flow STHE

(Adopted from Incopera *et.al*., 2007)

In *cross flow* STHE (*Figure 5*), the two fluid streams travel roughly perpendicular to one another.

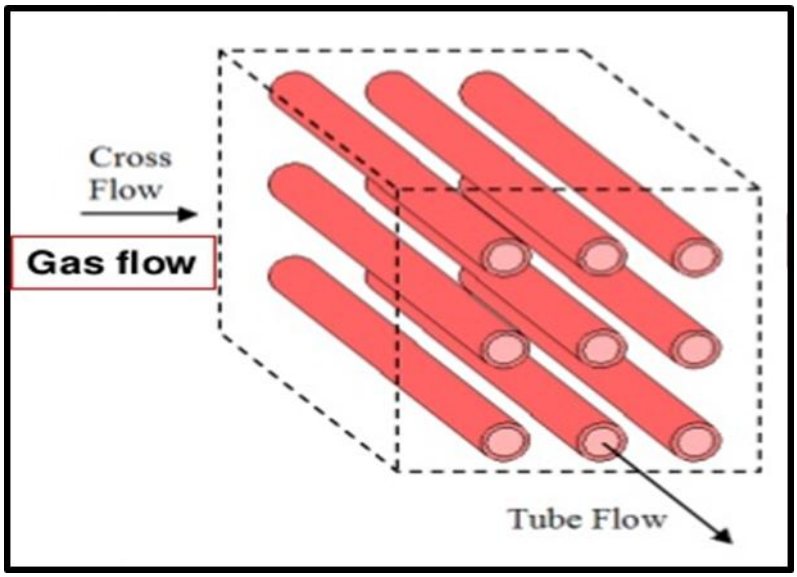

Figure 5. Flow arrangement for cross flow STHE

(Adopted from Incopera *et.al*., 2007)

2.1.3 Heat Exchanger Design Models

The design of a heat exchanger (HE) refers to its sizing. Sizing involves evaluating the tube and shell material, flow arrangement, exchanger construction type and physical size to meet the specification required by a process. The design of heat exchanger is based on the Kern Method, Bell-Delaware Method and the Tinker Method.

Kern (1950) gave a simple procedure for computing the shell-side pressure drop and heat transfer coefficient. However, the proposed method had the restriction that it would only serve for a fixed baffle cut (25%) and could not adequately account for baffle-to-shell and tube-to-baffle leakage. The Kern (1950) equation provides for a simple and quick calculation of shell-side heat transfer coefficient and pressure drop.

Tinker (1951) came up with a method that considered the various streams through the exchanger. He proposed a "stream analysis method" that incorporated schematic flow pattern. This included dividing the shell-side flow into a number of distinct streams. This method, however, was characterized by the use of rigorous iterative methodology and was deemed most appropriate for computer calculations rather than manual calculation. The shortcomings of this method led to the development of the Bell-Delaware Method (Bell, 1963). It used the theory of Tinker model

(1951) but revised it to be more suitable for manual design. Bell introduced correction factors that were based on extensive experimental data. For manual design, Saunders (1988) proposed the use of simple design factors for a fixed set of parameters. This made the Bell method more practical.

The research trend in the last decade has moved towards modeling and simulation with the inception of computers and programming, Reppich and Zagermann (1995) developed a computer-based heat exchange design model. They sought to determine the optimum dimensions of segmentally baffled shell-and-tube heat exchangers by calculating shell-side and tube-side pressure drops from the already existing Bell (1963) equations. The parameters that were studied were: shell diameter, number of baffles, tube length, baffle spacing, number of tubes and baffle cut. Their proposed model was also able to carry out cost analysis. He and Zhang (2001) conducted a theoretical analysis based on the Bell (1963) approach and an experimental test on a shell and tube latent heat storage exchanger. The results of the theoretical analysis model on the performance of the heat storage exchanger were found to be realistic and in agreement with experimental measurements.

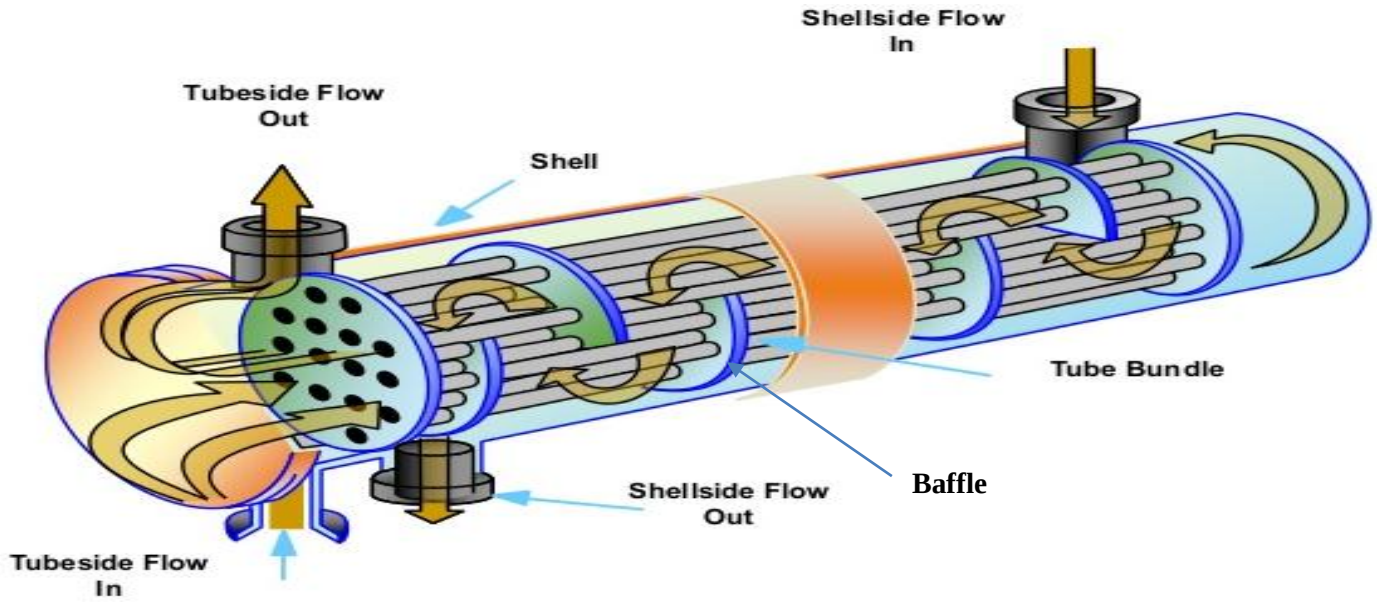

Figure 6. Shell and tube heat exchanger (STHE) Components

(Adopted from Mukherjee, 1992)

The evaluation of the impact of various parameters on the performance of STHE has been made easier by Computational Fluid Dynamics (CFD). Dirkse et al. (2006) modeled an STHE based on natural convection using CFD. Karno and Ajib (2005) developed software capable of calculating,

simulating and optimizing STHE design problems. The program analyzed the impact of shell size, baffle spacing, shell passes, tube size, baffle cut and tube length on the overall heat exchange transfer coefficient, thermal performance and efficiency. Joydeep *et.al*.,(2007) employed the use of Matlab simulation based on Kern Method (1950) to study the behavior of thermal (heat) exchangers by varying constraints such as baffle spacing, shell passes and baffle cut. The results showed that by varying the constraints, the heat exchange transfer coefficient also changed. The computed values and the literature values were observed to be in good agreement. Adelaja *et al.,* (2011) wrote a program using Visual Basic software that utilizes the Kern Method (1950) to evaluate the coefficients of heat transfer and the pressure drops in STHE. Previous works were focused on the thermo-hydraulic design of STHE but the developed program also incorporated the mechanical design. In an effort to increase the performance of STHE, Thundi *et al.* (2012) observed that by increasing the angle of inclination of the baffle, the heat transfer rate also increased; however, it led to a rapid drop in pressure. Kumaresan *et.al.,* (2017) investigated the effect of tilting the baffle angle and varying the baffle cuts on the STHE pressure drop and heat transfer rate using the CFD Ansys Fluent package. He considered baffle inclines of 25^0, 30^0, 35^0 and 40^0 for different baffle cuts of 35%, 25% and 30% of the shell inner diameter. His finding concluded that inclined baffle angles have high rates of heat transfer but also lead to higher pressure drops. The baffle incline angle of 30^0 and 30% baffle cut provided a higher rate of heat transfer without significant pressure drops. Hasu *et.al.,* (2017) also used the CFD Ansys software tool to model and simulate the effect of inclined helical baffles on the heat transfer rate. The simulation showed how the pressure varied in the shell due to the different helical inclinations and flow rates. Higher rates of heat transfer were also observed. He concluded that CFD was an effective design tool that allowed for implementation of design iterations to investigate the influence of different design parameters without tedious manual calculations.

Literature has shown that the Kern model coupled with computer simulation is an effective tool in the design and optimization of heat exchangers.

Chapter Three

Materials and Methods

The proposed thermal desalination system works as follows: preheated saline water from the solar heating system is passed through an atomizer where it is broken down into small droplets by electric force. The small droplets create a large surface area for evaporation. The moist air formed in the evaporation chamber is then drawn out by a suction fan and directed into the condenser (*Figure 7*) which is supplied with water from the cooling tower. The water vapor then condenses on the cold tubes thus forming distilled water which is collected and treated to make it suitable for drinking.

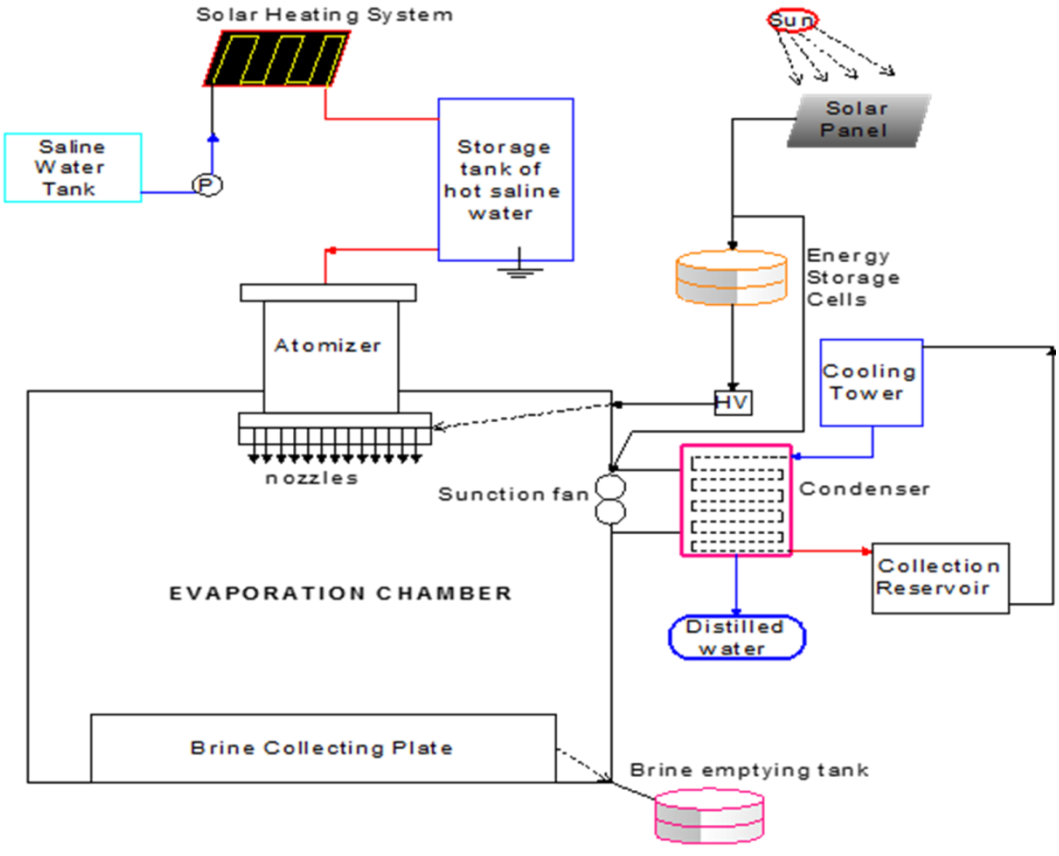

Figure 7. The Schematic flow diagram of the proposed thermal desalination system

This research study focused on the condensation system for the water vapor from the evaporation chamber. It comprised of: the sizing of the condenser (*section 2.3*) using the Kern Method (Kern, 1950); simulation of the condensation system using Matlab-Simulink program to predict the performance of the system under different conditions; fabrication of the condenser; performing experiments and validation analysis.

3.1 Acquisition of the Input Parameters

A fabricated experimental evaporation chamber (diameter 62 cm, height 82 cm) was fitted, at the top, with a digital hygrometer to measure the temperature and relative humidity (RH) of the moist air from the evaporation chamber. To validate the hygrometer temperature readings, a temperature probe Model no. ALTZD was also used. A circular opening of 10.5 cm in diameter, fitted with a suction fan (*Figure 7*), was made at the upper part of the evaporation chamber and served as the pathway of the moist air from the chamber to the condenser. To find out the evaporation efficiency, a mass balance was carried out. It was done by calculating the difference between the amounts of water put into the evaporation system and the amount of water collected at the bottom of the chamber (brine) over a specified period of time. This also gave the mass flow rate of the water-vapor (m_s).

3.2 Model Design

The Kern Method (Kern, 1950) was used for the design of the condenser using the algorithm in Figure 8. The method involved evaluating tube and shell heat transfer coefficients, baffle spacing and cut, the tube and shell materials, flow arrangement, exchanger construction type and physical size of the exchanger to meet the specification required.

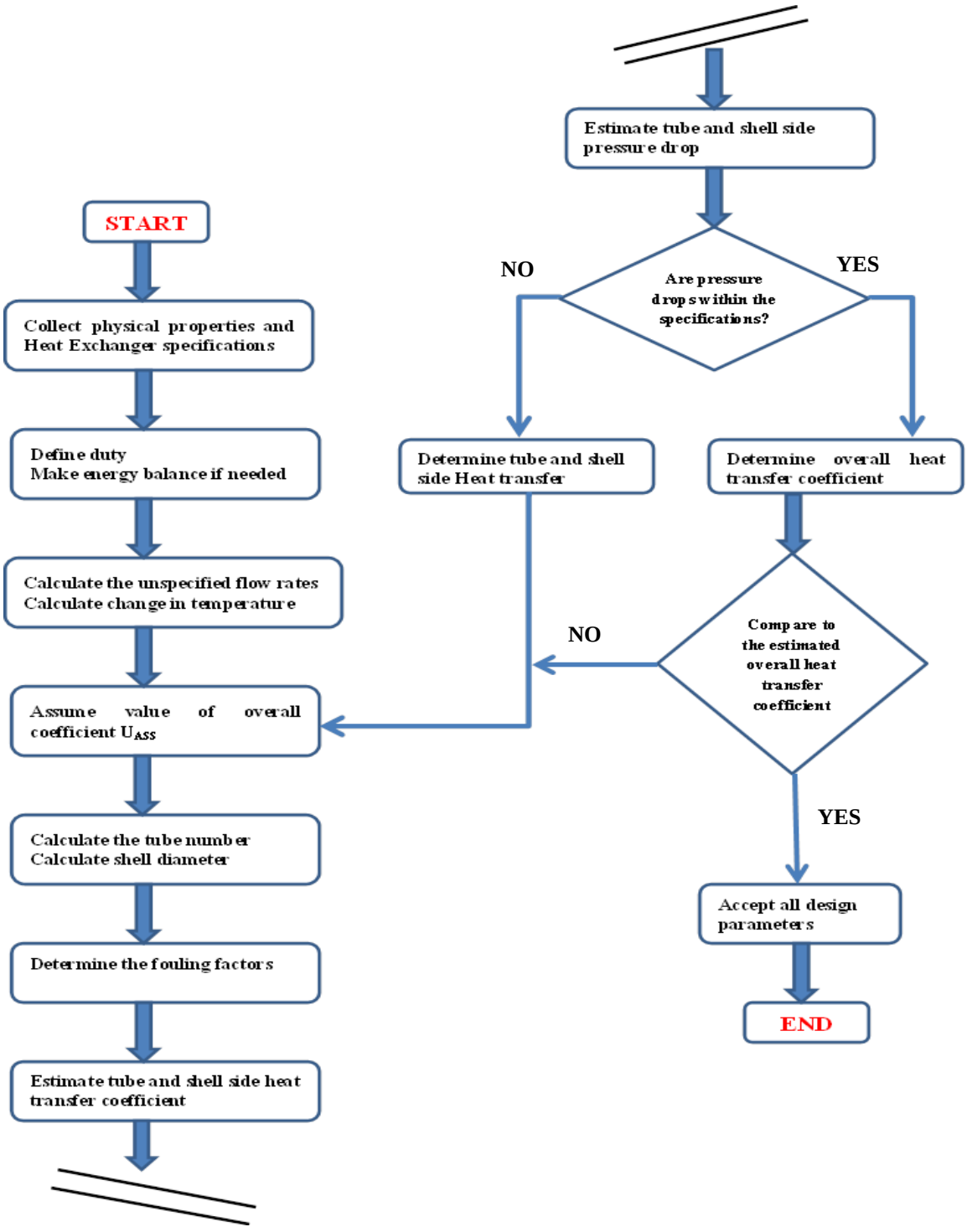

Figure 8. Algorithm of the design procedure (Kern,1950)

3.2.1 Collection of Physical Properties and Heat Exchanger Specifications

The physical properties of the water and moist air were obtained from literature and tabulated. The properties that were of interest were: density, enthalpies, viscosity and specific heat (*Appendix 1*).

A cross-flow STHE (Figure 5) was chosen as the most suitable since it is typically applied in situations where one of the fluid streams is a gas and the other a liquid as was the case in this research. As required by the Kern Method (Kern, 1950) the choice of the tube arrangement needed to be made. Tubes in a heat exchanger can be arranged in triangular, square, or rotated square pattern. The rotated square pattern tube arrangement was chosen as it allowed for higher heat transfer rates.

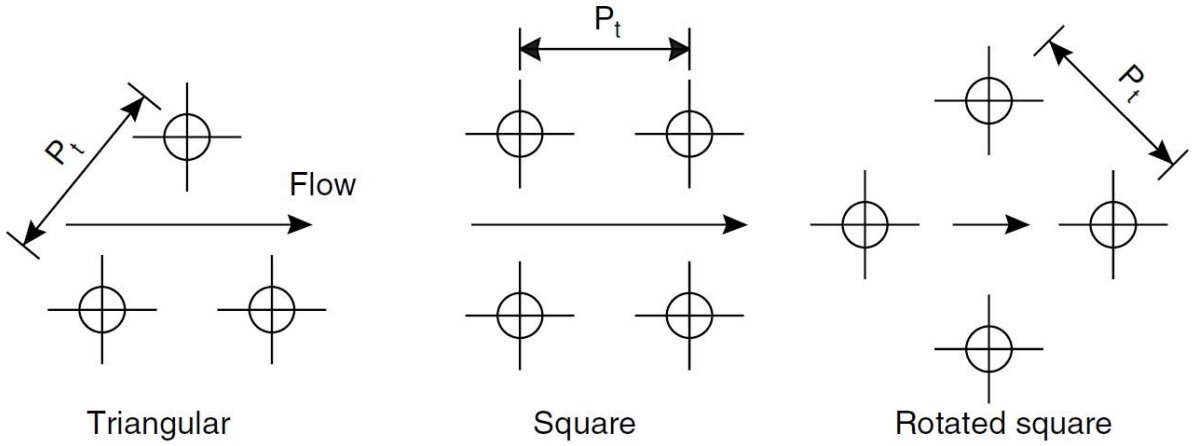

Where P_t is the pitch and it denotes the distance between the centres of two adjacent tubes.

Figure 9. Tube arrangement patterns (Adopted from Coulson *et.al*, 1999)

3.2.2 Determination of Heat Exchange Rate (Duty)

The heat exchange rate was determined using the following equation:

$$Q\,(W) = \acute{m}_S * h \quad \ldots\ldots\ldots\ldots\ldots\ldots\ldots\ldots\ldots\ldots\ldots\ldots\ldots\ldots\ldots\ldots\ldots\ldots\ldots\ldots\ldots\ldots 3.1$$

Where Q is the heat exchange rate in watts, $\acute{m}_S$ is the mass flow rate of the moist air in kg s^{-1} and h is the enthalpy of the moist air in J Kg^{-1} *()*.

An energy balance was done to determine the unknown temperature difference of the cooling water using equation 3.2b. To determine m_w the recommended range of 1.5 – 4.0 m s^{-1} of water

velocities for flow in tubes of STHE together with the recommended tube diameters (*section 3.2.4*) were used (Coulson *et.al*,, 1999).

$$m_w = \rho * A * V \quad \text{.....3.2a}$$

$$Q\,(W) = \acute{m}_S * h = m_w * c_p * \Delta T \quad \text{.....3.2b}$$

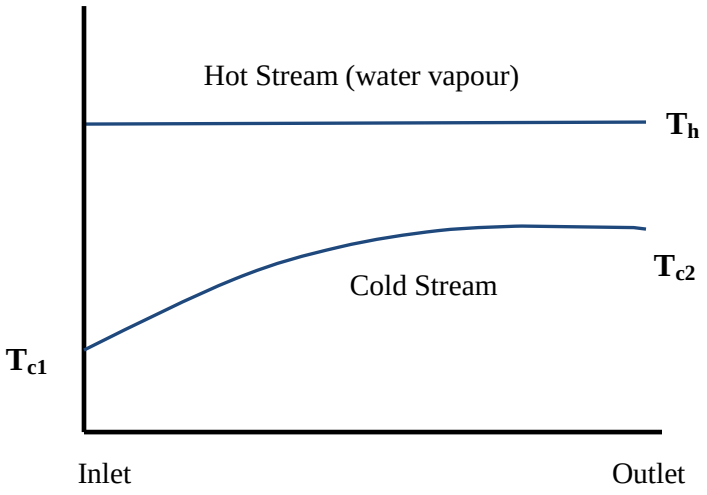

Figure 10. Temperature distribution in the heat exchanger

Where m_w is the mass flow rate of the cooling water in the tubes, c_p is the specific heat of water in J Kg^{-1} K^{-1}; ΔT is the temperature difference between the inlet Temperature and outlet temperature of the cooling water as it enters and leaves the condenser; ρ is the density of water in kg m^{-3}; A is the cross sectional area of the tube (m^2) (*discussed in section 3.2.4*) and V is the velocity of the cooling water in m s^{-1}(Coulson *et.al*, 1999).

T_{c1}, T_{c2} and T_h in figure 10 were used to denote the inlet and outlet temperatures of the cooling water and temperature of the hot moist air respectively (Figure 10). T_{c1} was set to 18^0C (the wet-bulb temperature as measured by experiments) and using the temperature difference (ΔT) calculated from equation 2, T_{c2} could be determined.

The Kern Method (Kern, 1950) requires that the Logarithmic Mean Temperature Difference (LMTD) is calculated and used to determine the area of the STHE. This was obtained from the equation below (Coulson *et.al*, 1999);

$$T_{LMTD} = \frac{T_{c2} - T_{c1}}{In\left(\frac{T_h - T_{c1}}{T_h - T_{c2}}\right)} \quad \text{.....3.3}$$

3.2.3 Assumption of value of Overall Co-efficient, U_{ass}

The Kern Method (Kern, 1950) is an iterative process. To start the iteration the method recommends that an assumed value of Overall Coefficient, U_{ass} is from empirical overall coefficients of Heat Exchangers (Figure 11). The value of 1000 W m^{-2} K^{-1} was selected from the range highlighted in figure 11 to start the iteration.

Shell and tube exchangers

Hot fluid	Cold fluid	*U* (W/m² °C)
Heat exchangers		
Water	Water	800–1500
Organic solvents	Organic solvents	100–300
Light oils	Light oils	100–400
Heavy oils	Heavy oils	50–300
Gases	Gases	10–50
Coolers		
Organic solvents	Water	250–750
Light oils	Water	350–900
Heavy oils	Water	60–300
Gases	Water	20–300
Organic solvents	Brine	150–500
Water	Brine	600–1200
Gases	Brine	15–250
Heaters		
Steam	Water	1500–4000
Steam	Organic solvents	500–1000
Steam	Light oils	300–900
Steam	Heavy oils	60–450
Steam	Gases	30–300
Dowtherm	Heavy oils	50–300
Dowtherm	Gases	20–200
Flue gases	Steam	30–100
Flue	Hydrocarbon vapours	30–100
Condensers		
Aqueous vapours	Water	1000–1500
Organic vapours	Water	700–1000
Organics (some non-condensables)	Water	500–700
Vacuum condensers	Water	200–500
Vaporisers		
Steam	Aqueous solutions	1000–1500
Steam	Light organics	900–1200
Steam	Heavy organics	600–900

Figure 11. Empirical Overall Heat Transfer coefficients (Adopted from Coulson *et.al*, 1999)

3.2.4 Determination of the Tube Number and Shell Diameter

Figure 12 shows the overall diagram of a STHE. It also shows the different components that constitute a STHE system.

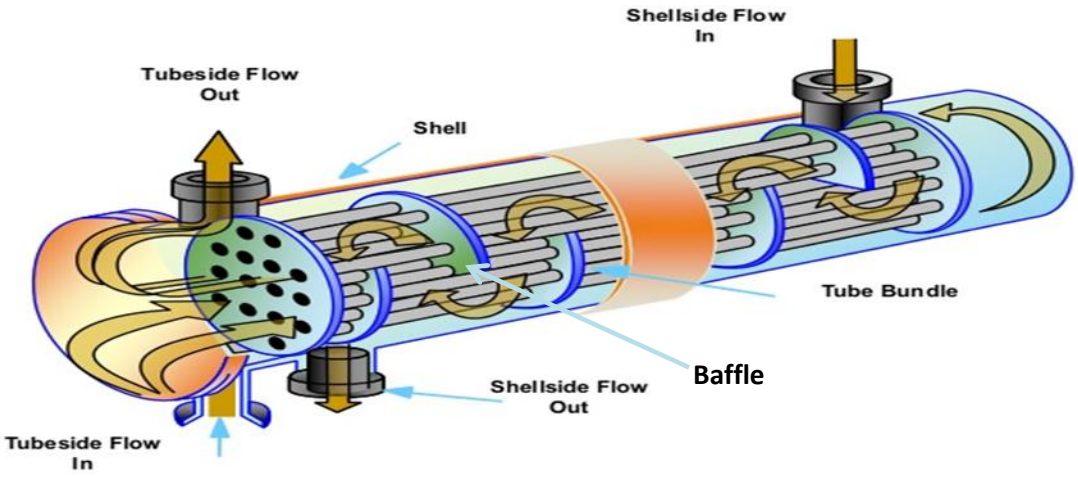

Figure 12. Shell and Tube Heat Exchanger (STHE) components
(Adopted from Mukherjee, 1992)

STHE systems can have multiple tube passes in their flow arrangements. This denotes the number of times the tube side fluid (in our case the cooling water) goes through the tubes. Figures 13a and 13b show the flow arrangements in a single tube and two-tube pass STHE respectively. The two-tube pass STHE was chosen as it lengthens the time of the tube side fluid in the heat exchanger allowing for higher heat exchange rates.

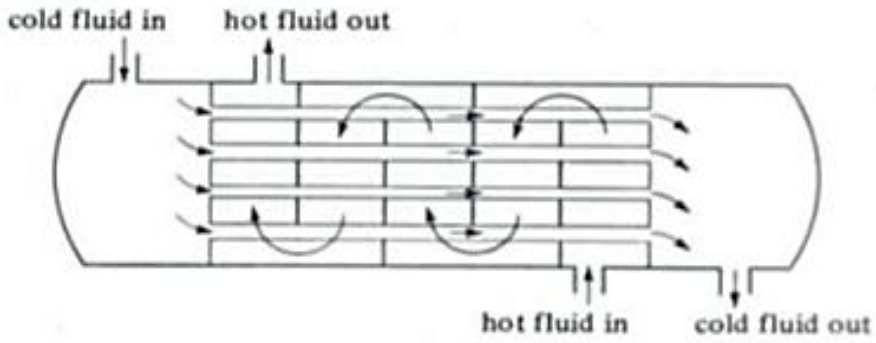

Figure 13a. Single tube pass flow arrangement for STHE (Adopted from Incopera *et.al*., 2007*)*

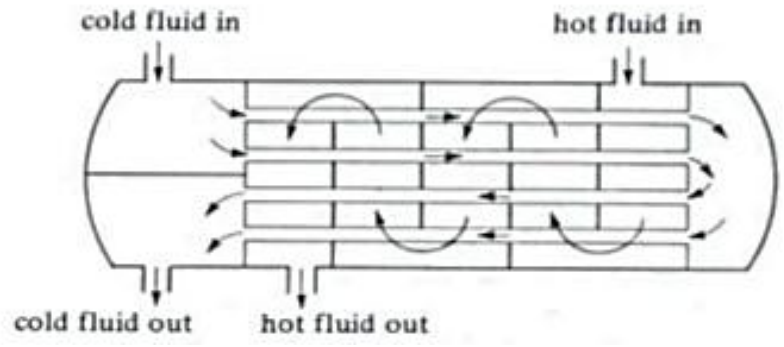

Figure 13b. Two-tube pass flow arrangement for STHE (Adopted from Incopera *et.al*., 2007)

To evaluate the area needed to satisfy the heat exchange rate specified by Equation 3.1, the relationship below was used:

$$Q\,(W) = \acute{m}_S * h = m_w * c_p * \Delta T = A * U_{ass} * T_{LMTD} \quad \ldots\ldots\ldots\ldots\ldots\ldots\ldots\ldots 3.4$$

Where A is the area in m^2, U_{ass} is the empirical overall heat transfer coefficient and T_{LMTD} is the Logarithmic Mean Temperature Difference (*equation 3.3)* (Coulson *et.al*, 1999).

The recommended diameters of heat exchanger tube are in the range of 16 mm to 50 mm for the outer diameter (OD) (Coulson *et.al*, 1999). The 16 mm (OD) copper tube diameter was chosen since smaller tubes give a larger surface area for heat transfer. The number of tubes required was obtained by dividing the area, A (*equation 3.4*) by the surface area of one tube and the distance between the tubes was defined by the pitch (Figure 9). The recommended pitch is 1.25 times the tube's outer diameter (OD) i.e. $1.25D_o$ (Coulson *et.al*, 1999).

To define the shell diameter (Figure 12) for a two-tube pass, the tube bundle was first determined. The empirical formula for this is:

$$D_b = D_O\left(\frac{N_t}{K_1}\right)^{\frac{1}{n_1}} \quad \ldots\ldots\ldots\ldots\ldots\ldots\ldots\ldots 3.5$$

Where D_b is the bundle diameter in mm, D_o is the tube outside diameter in mm, N_t is the number of tubes and K_1 and n_1 are constants (Coulson *et.al*, 1999).

Triangular pitch, $p_t = 1.25d_o$					
No. passes	1	2	4	6	8
K_1	0.319	0.249	0.175	0.0743	0.0365
n_1	2.142	2.207	2.285	2.499	2.675
Square pitch, $p_t = 1.25d_o$					
No. passes	1	2	4	6	8
K_1	0.215	0.156	0.158	0.0402	0.0331
n_1	2.207	2.291	2.263	2.617	2.643

Figure 14. Table of Constants K_1 and n_1 (Coulson *et.al*, 1999)

After determining the tube bundle diameter, the shell inside diameter was read off from the Shell-Bundle clearance chart (figure 15). The fixed and U-tube bundles are most preferred due to their relatively low maintenance and cost.

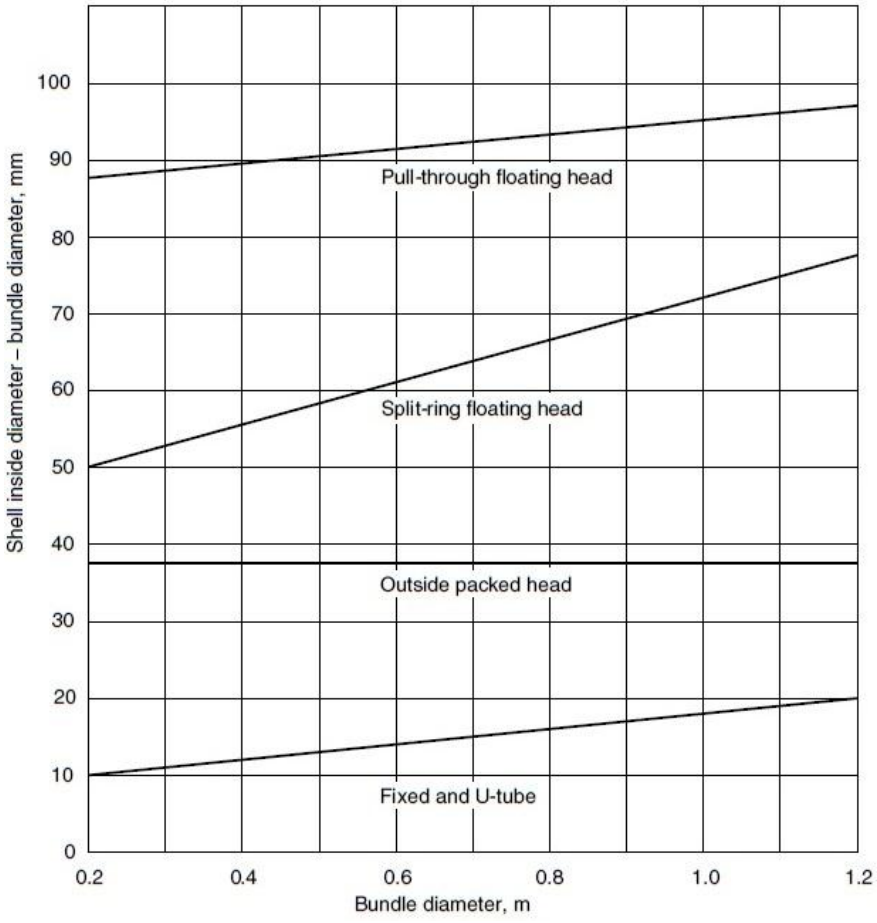

Figure 15. Shell-Bundle Clearance Chart (Coulson *et.al*, 1999)

Once the shell diameter was determined, the next step was to define the tube length and baffle design and spacing. The recommended ratio of tube length to shell diameter is in the range of 5-10 (Coulson *et.al*, 1999). Baffles (Figure 12) are used to direct the flow of the shell side fluid over the tube bundle, increasing velocity and turbulence so as to achieve higher heat transfer rates. They also help support the tubes against sagging and vibrations caused by fluid flow eddy. There are different types of baffles but the segmental baffles are the most common since they allow for easy construction of the heat exchanger. The baffle spacing according to recommendations should not be closer than 20% of the shell inside diameter (Coulson *et.al*, 1999).

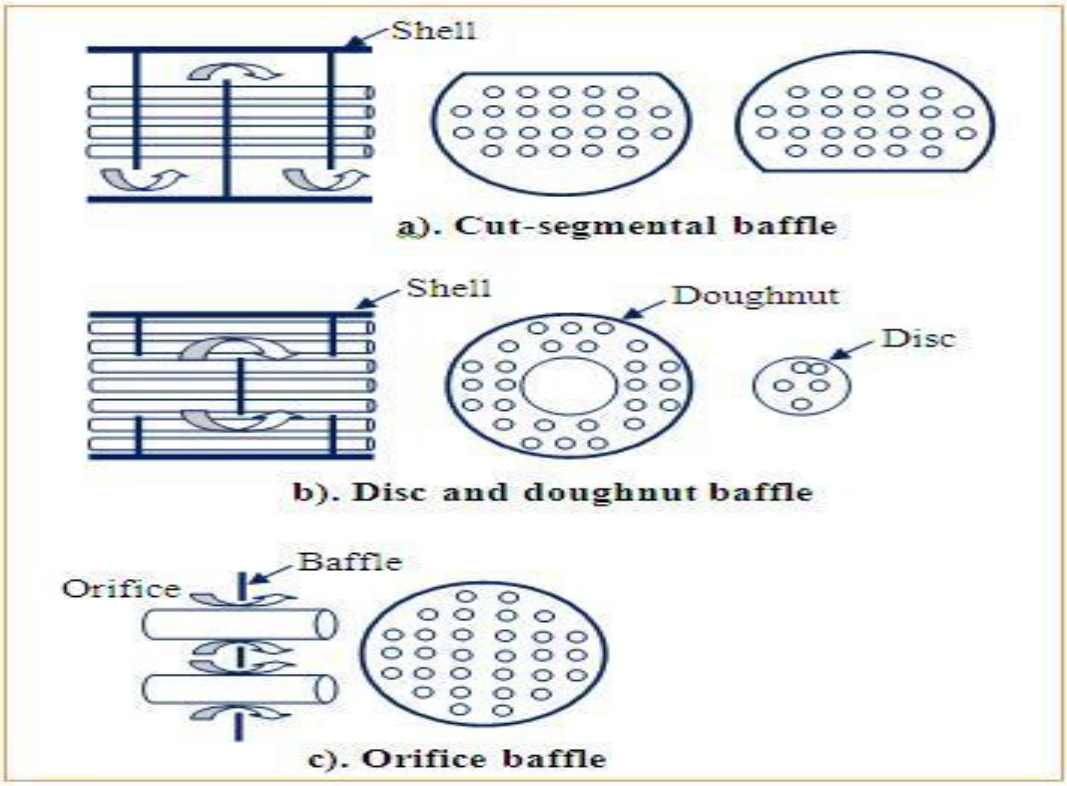

Figure 16. Different types of baffles (Coulson *et.al*, 1999)

3.2.5 Estimation of the Tube Side Heat Transfer Coefficient (h_i)

This coefficient defines the rate at which a moving fluid (in our case cooling water) will transfer heat to the tube.

To determine h_i, the Nusselt relationship was used:

$$\frac{h_i * d_i}{k_f} = j_h * Re * Pr^{0.33} \quad \text{.....3.6}$$

Where h_i is the tube side heat transfer coefficient in W m^{-2} K^{-1}; d_i is the tube inside diameter, mm; k_f is the fluid thermal conductivity, W m^{-2} K^{-1}; j_h is the heat transfer factor based on tube dimensions; Re is the Reynolds number, dimensionless; Pr is the Prandtl number, dimensionless, (Coulson *et.al*,1999).

The Reynolds and Prandtl numbers are defined using the equations below:

$$Re = \frac{\rho V d_i}{\mu} \quad \text{.....3.7a}$$

$$Pr = \frac{C_p * \mu}{k_f} \quad \text{.....3.7b}$$

Where ρ is the density of water in kg m^{-3}, V is the flow velocity in m s^{-1}, d_i is the tube inner diameter in m, C_p is the specific heat capacity of water in J kg^{-1} K^{-1}, μ is the dynamic viscosity in kg m^{-1} s^{-1}, and k_f is the fluid thermal conductivity in W m^{-2} K^{-1}(Coulson *et.al*, 1999). The heat transfer factor j_h was read off from the chart below (Figure 17). The ratio of the tube length (L) to the tube diameter (D_o) (*section 3.2.4*) is required to identify which of the graphs in the chart is to be used.

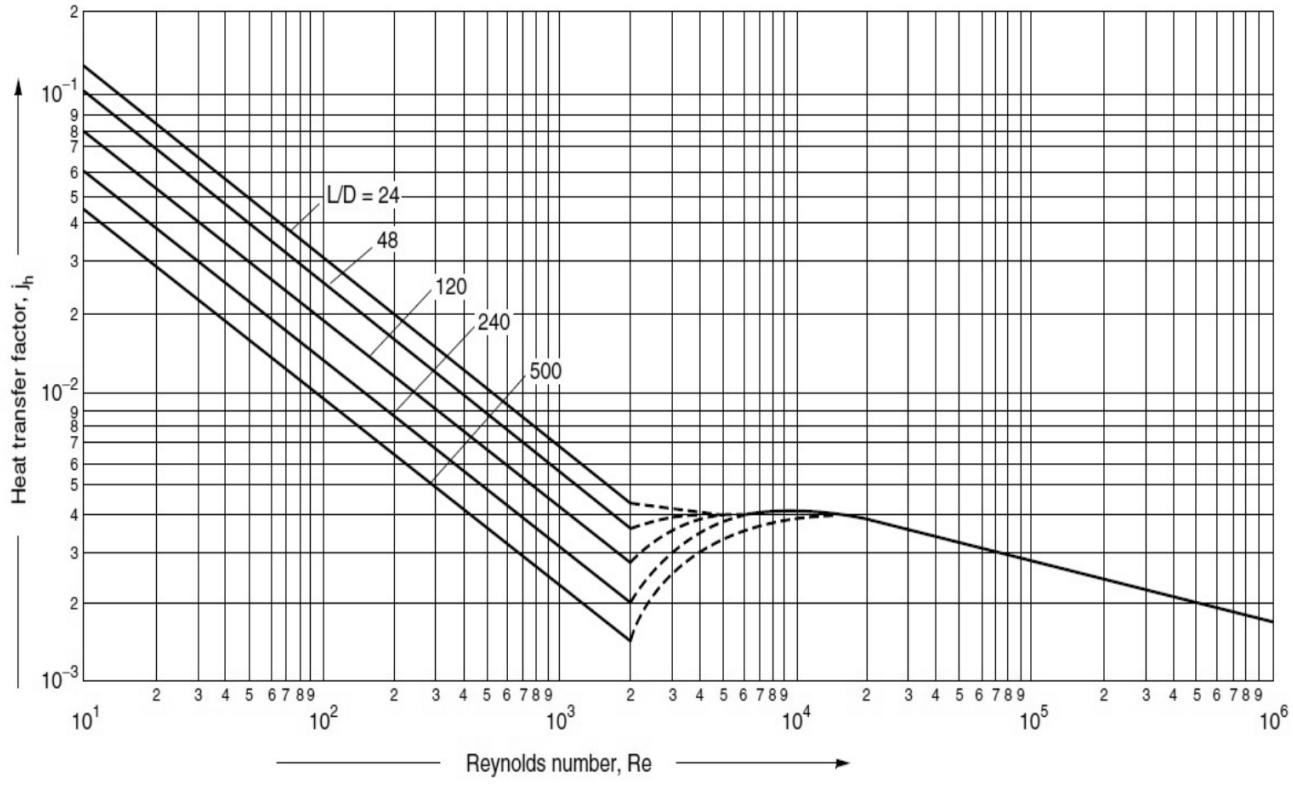

Figure 17. Heat transfer factor (j_h) chart (Coulson *et.al*, 1999)

3.2.6 Estimation of Shell Side Heat Transfer Coefficient (h_o)

It defines the rate at which shell side fluid (case of moist air) will transfer heat to the surface of tube.

This was determined from the following empirical formula for condensation on horizontal tube bundle:

$$h_o = 0.95k_l\left(\frac{\rho_l(\rho_l-\rho_v)g}{\mu_l\Gamma}\right)^{\frac{1}{3}} \quad \text{.....3.8}$$

Where h_o is the shell side heat transfer coefficient (condensation film) coefficient in W m^{-2} K^{-1}; k_l is the condensate (water) thermal conductivity in W m^{-1} K^{-1}; ρ_l is the condensate (water) density in kg m^{-3}; ρ_v is the vapor density in kg m-3; μ_l is the condensate(water) dynamic viscosity in kg m^{-1} s^{-1}; g is the gravitational acceleration, that is 9.81 m s^{-2} and Γ is the tube loading, i.e. the condensate flow per unit length of tube in kg m^{-1} s^{-1} (Coulson *et.al*, 1999).

3.2.7 Determination of the Overall Heat Transfer Coefficient (U_o)

The Overall Heat Transfer Coefficient was determined using the equation below:

$$\boldsymbol{U_o = \frac{1}{(r_o/r_i)\frac{1}{h_i} + (r_o/r_i)R_{fi} + \frac{r_o}{k_c}\, In\,(r_o/r_i) + R_{fo} + \frac{1}{h_o}}} \quad \text{.....3.9}$$

Where r_o and r_i are the outer and inner radius of the tube respectively in m; k_c is the thermal conductivity of the tube material in W m^{-1} K^{-1}; fouling factors represents the resistance to heat flow due to a build-up of a layer of dirt, R_{fi} is the fouling factor for the inside of the tube due to the flow of cooling water in m^2 K $W^{-1}$and R_{fo} is the fouling factor for the outside of the tube due to the water vapor flowing over the tubes in m^2 K W^{-1}(Coulson *et.al*, 1999). The fouling factors were obtained from the table below.

Fluid	Coefficient ($W/m^2 °C$)	Factor (resistance) ($m^2°C/W$)
River water	3000–12,000	0.0003–0.0001
Sea water	1000–3000	0.001–0.0003
Cooling water (towers)	3000–6000	0.0003–0.00017
Towns water (soft)	3000–5000	0.0003–0.0002
Towns water (hard)	1000–2000	0.001–0.0005
Steam condensate	1500–5000	0.00067–0.0002
Steam (oil free)	4000–10,000	0.0025–0.0001
Steam (oil traces)	2000–5000	0.0005–0.0002
Refrigerated brine	3000–5000	0.0003–0.0002
Air and industrial gases	5000–10,000	0.0002–0.0001
Flue gases	2000–5000	0.0005–0.0002
Organic vapours	5000	0.0002
Organic liquids	5000	0.0002
Light hydrocarbons	5000	0.0002
Heavy hydrocarbons	2000	0.0005
Boiling organics	2500	0.0004
Condensing organics	5000	0.0002
Heat transfer fluids	5000	0.0002
Aqueous salt solutions	3000–5000	0.0003–0.0002

Figure 18. Typical fouling factors for different fluids (Coulson *et.al*, 1999)

3.2.8 Comparison of the Determined Overall Heat Transfer Coefficient (U_o) with the Assumed overall heat transfer coefficient (U_{ass})

The determined overall heat transfer coefficient (U_o) (*equation 3.9*) was compared with the assumed overall heat transfer coefficient (Uass) (*section 3.2.3*). If there was a wide variance between the two, the procedure outlined above was repeated until an optimal solution was arrived at.

3.3 Fabrication of the Condenser

Following the model specifications (*section 3.2*), copper tubes of outer diameter (OD) $16x10^{-3}$ m and inner diameter $14x10^{-3}$ m (ID) were used for the fabrication of the condenser. The shell and the baffles (*Figure 12*) were made of aluminium sheet (gauge 22). Both of these materials were chosen due to their good thermal conductivities and availability in the local market.

3.4 Experimentation

After the fabrication of the condenser, it was attached to the upper part of the evaporation chamber (Figure 7) and experiments were carried out. The moist air from the evaporation chamber was directed into the condenser. The moist air travels through the condenser and gets into contact with the copper tubes. The cold water flows through the copper tubes. The water vapor then condenses on the cold surface of the copper tubes. The amount (mass) of the condensate from the experiments was then collected and measured.

3.5 Simulation of the STHE using Matlab program

Section 3.2 defines the Kern modelling process. The parameters obtained from the Kern model were used to simulate the performance of the STHE under different conditions.

The Matlab-Simulink program was used to simulate the working of the designed STHE. A library called Thermolib was added on to Matlab-Simulink software to enable the program performs thermodynamic processes. The parameters [shell diameter, tube diameter, shell side and tube side heat transfer coefficients and the overall heat transfer coefficient] obtained from the Kern model (Kern, 1950) were fed into the program as input parameters. The simulation was carried out to predict the performance of the condenser under varying conditions of relative humidity [70%, 50% and 40%] and inlet cooling water temperatures, (T_{c1}), [5^{O}C, 10^{O}C, 15^{O}C and 20^{O}C]. The conditions selected were based on the experiments. The simulation generated performance curves that predicted the efficiency of the condenser, the amount of condensed water and outlet cooling water temperature (T_{c2}) under the different conditions.

3.6 Validation of the Model

The results from the experiments were compared with the results from the simulation done using Matlab-Simulink software.

Chapter Four

Results and Discussion

4.1 Kern Model

Following the steps outlined in *section 3.2* an excel worksheet was made that gave the results of the iterative Kern modeling process (Kern, 1950) until an optimal solution was achieved (*refer to Appendices*). The iterations were done at different cooling water velocities. The recommended water velocity in tubes for STHE is in the range of 1.5 – 4.0 m s^{-1} with the maximum value of 4.0 m s^{-1} used when fouling needs to be reduced (Coulson *et.al*, 1999). At each of the velocities, the mass flow rate (m_w) of the cooling water was calculated and from the energy balance equation (*equation 3.4*), an Assumed Overall Heat Transfer Coefficient (U_{ass}) was taken. The recommended range of the U_{ass} is 1000 – 1500 W $m^{-2}K$ (*Figure 11*) (Coulson *et.al*, 1999). To start the iteration, 1000 (W $m^{-2}K$) was selected. At U_{ass} of 1000 (W $m^{-2}K$), the Overall Heat Transfer Coefficient (U_o) was determined. The aim was to get to a point where U_{ass} and the U_o showed little to no difference. Whenever a large difference between the two values was observed, the process would start again at a different U_{ass} value but within the recommended range (1000 – 1500 W $m^{-2}K$). The iterations were done at 1000, 1100, 1200, 1300, 1400 and 1500 W $m^{-2}K$ at each of the recommended water velocity range of 1.5 – 4.0 m s^{-1}. The water velocities that were considered included: 1.5, 2.0, 2.5, 3.0 and 4 m s^{-1}.

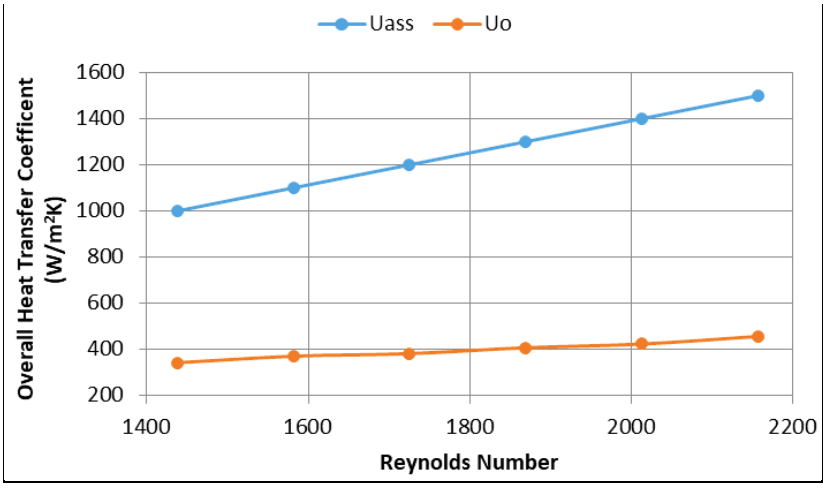

Figure 19a. Comparison between U_{ass} and U_o at a cooling water velocity of 1.5 m s^{-1}

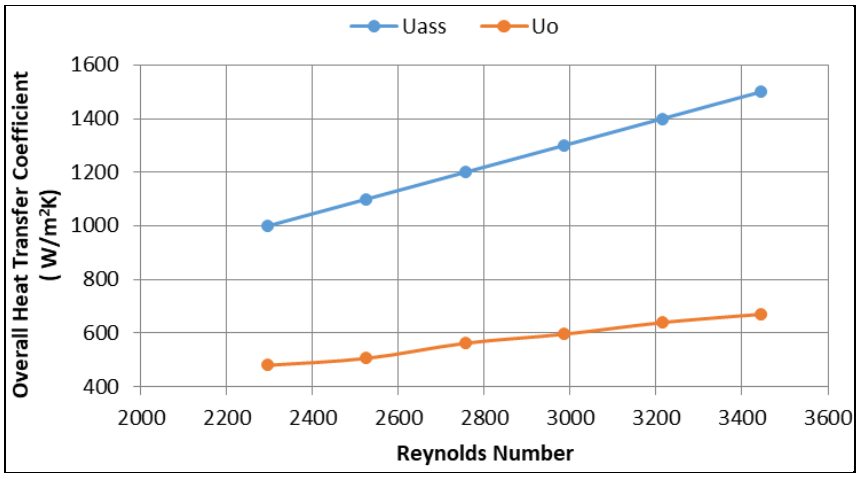

Figure 19b. Comparison between U_{ass} and U_o at cooling water velocity of 2.0 m s^{-1}

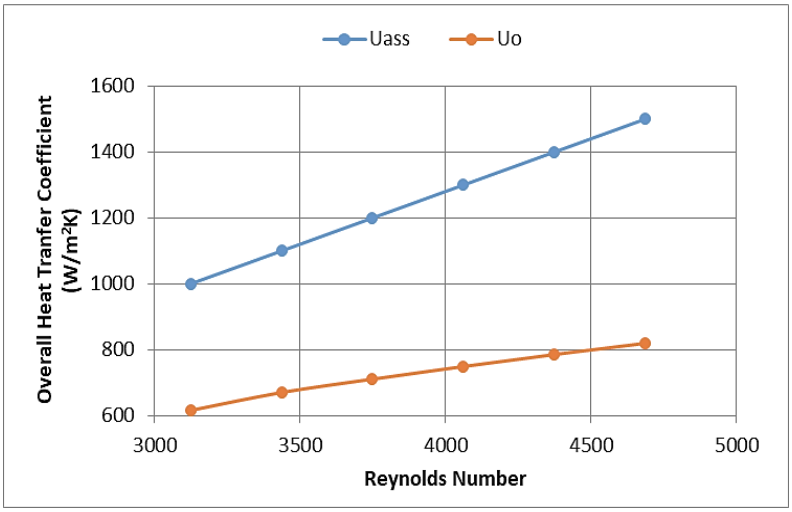

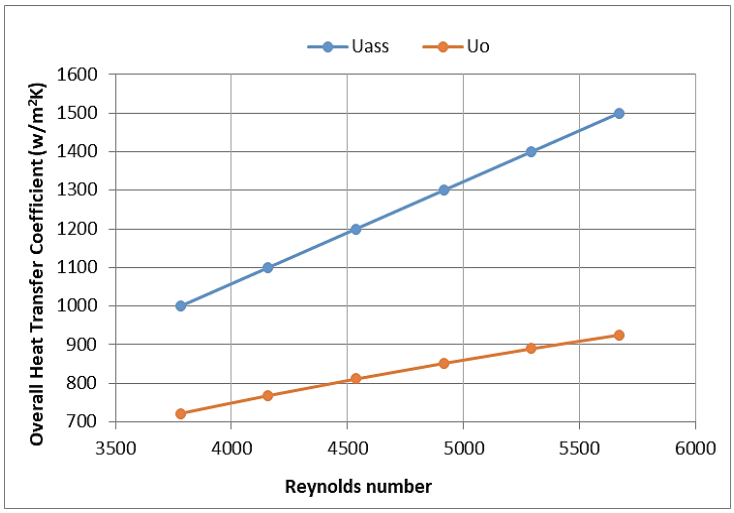

(19c) (19d)

Figure 19c & 19d. Comparison between U_{ass} and U_o at cooling water velocities of 2.5 and 3.0 m s^{-1} respectively

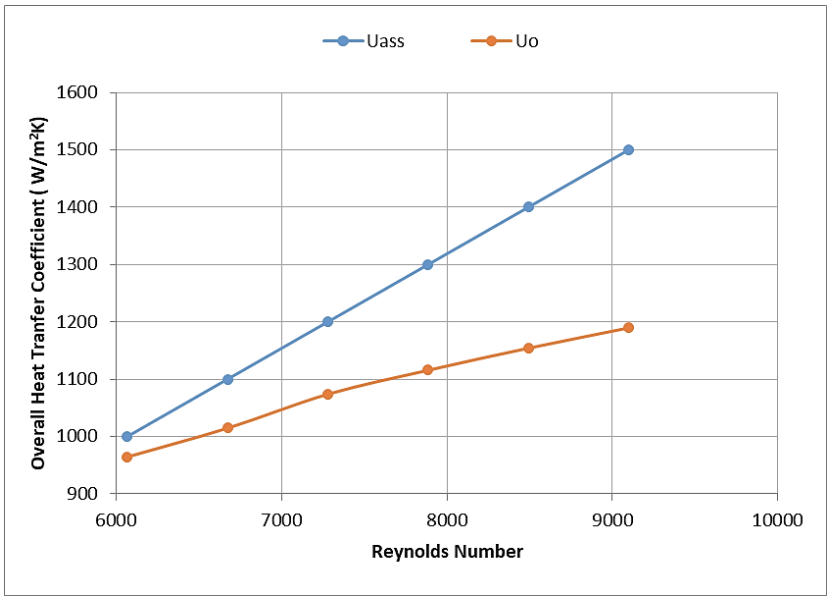

Figure 19e. Comparison between U_{ass} and U_o at Cooling Water Velocity of 4.0 m s^{-1}

Figures 19a to 19e show the comparison between U_{ass} and U_o in relation to the Reynolds number. The Reynolds number (Re) defines the flow regime in the tubes (*Figure 20*). Re value of over 4300 implies that the flow in the tubes is in the turbulent flow regime and Re value of below 2100 signifies a laminar flow. Laminar flow is characterized by low velocities where a fluid flows in a conduit in smooth layers with the inner layers flowing at higher rates than the outer layers (Coulson *et.al*, 1999). In STHE, the outer layers form an insulation thus lowering the heat transfer rates. In turbulent flow, the fluid is agitated and this causes rapid mixing in the fluid allowing for higher heat transfer rates. A Re value between 2100 – 4000 represents transitional flow regime where the flow is considered to be unstable. The preferred flow regime is turbulent flow due to higher rates of heat transfer.

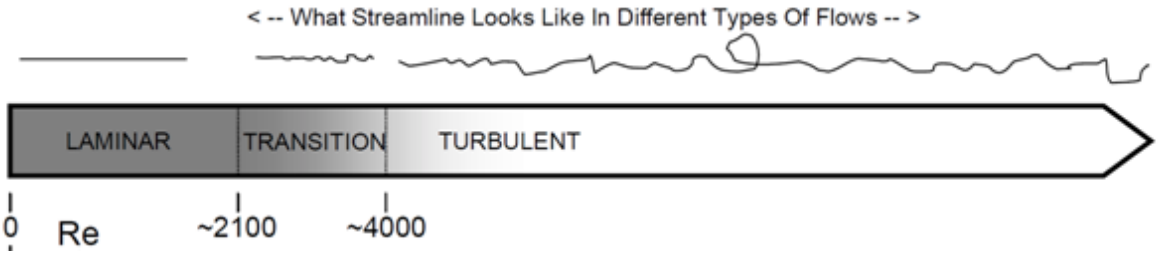

Figure 20. Flow regimes in pipes (Adopted from Incopera *et.al*., 2007)

The flows in Figures 19a and 19b are in the laminar flow regime. U_{ass} and U_o also show a large variance hence the design parameters are not optimal. Figures 19c & 19d represent flows of Reynolds number ranging from 3200 to 5700 (transition to turbulent flow).Where U_{ass} and U_o exhibit large differences implying that an optimal solution has not been achieved at. Figure 19e shows flow in the turbulent regime with Reynolds number > 6000. The graph also indicates that at U_{ass} = 1000 (W m^{-2} K^{-1}), U_o = 964 (W m^{-2} K^{-1}) and again, at U_{ass} = 1100 (W m^{-2} K^{-1}), U_o = 1015 (W m^{-2} K^{-1}) (*appendices*). The difference between U_{ass} and U_o is not big (~100 W m^{-2} K^{-1}). According to literature ((Coulson *et.al*, 1999)), this difference is acceptable and the design parameters here can therefore be used. The design parameters at U_{ass} of 1100 (W m^{-2} K^{-1}) were used for the fabrication of the condenser (*appendices*).

4.2 Fabrication of the Condenser

This section describes the fabrication of the condenser using the accepted design parameters in *section 4.1*.

At U_{ass} of 1100 (W m^{-2} K^{-1}) the physical design parameters (*section 3.2.4 and appendices*) were as follows:

Table 1. Showing the accepted design parameters at U_{ass} of 1100 (W m^{-2} K^{-1})

Physical Design Parameter	Value
Tube Cross-sectional area, m^2	$0.0002 * 10^{-1}$
Tube inner Diameter, D_i, in m	$0.14 * 10^{-1}$
Tube outer Diameter, D_o, in m	$0.16 * 10^{-1}$
Length of tube, m	$7.0 * 10^{-1}$
Number of Tubes, N_t	17
Pitch, P_t, in m	$0.2 * 10^{-1}$
Bundle Diameter, D_b, in m	$1.0 * 10^{-1}$
Shell Diameter, m	$1.2 * 10^{-1}$

Baffle Spacing, in m	$1.4*10^{-1}$
Number of Baffles	5

The tubes were made of copper and the shell of aluminium gauge 22 (Figure 21). The materials were chosen due to their availability in the local market and high rates of heat transfer (thermal conductivity of Copper and Aluminium is 401 and 200 W m^{-1} K^{-1}).

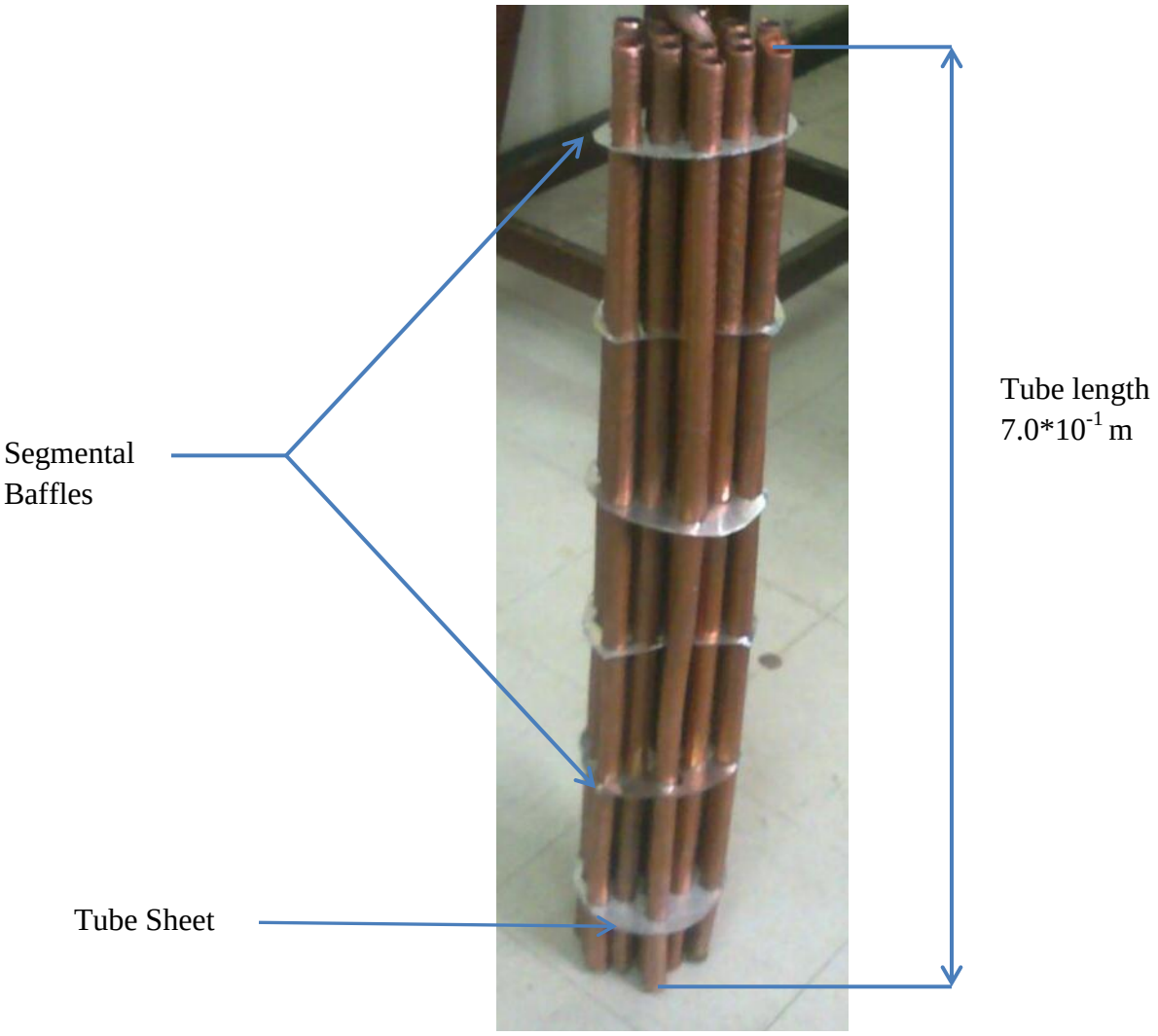

Figure 21. The fabricated condenser without the shell cover

4.3 Experimental Results

Following its successful fabrication (*section 4.2*), the condenser was then attached to the evaporation chamber to run the experiments. The experimental set-up is shown in figure 22.

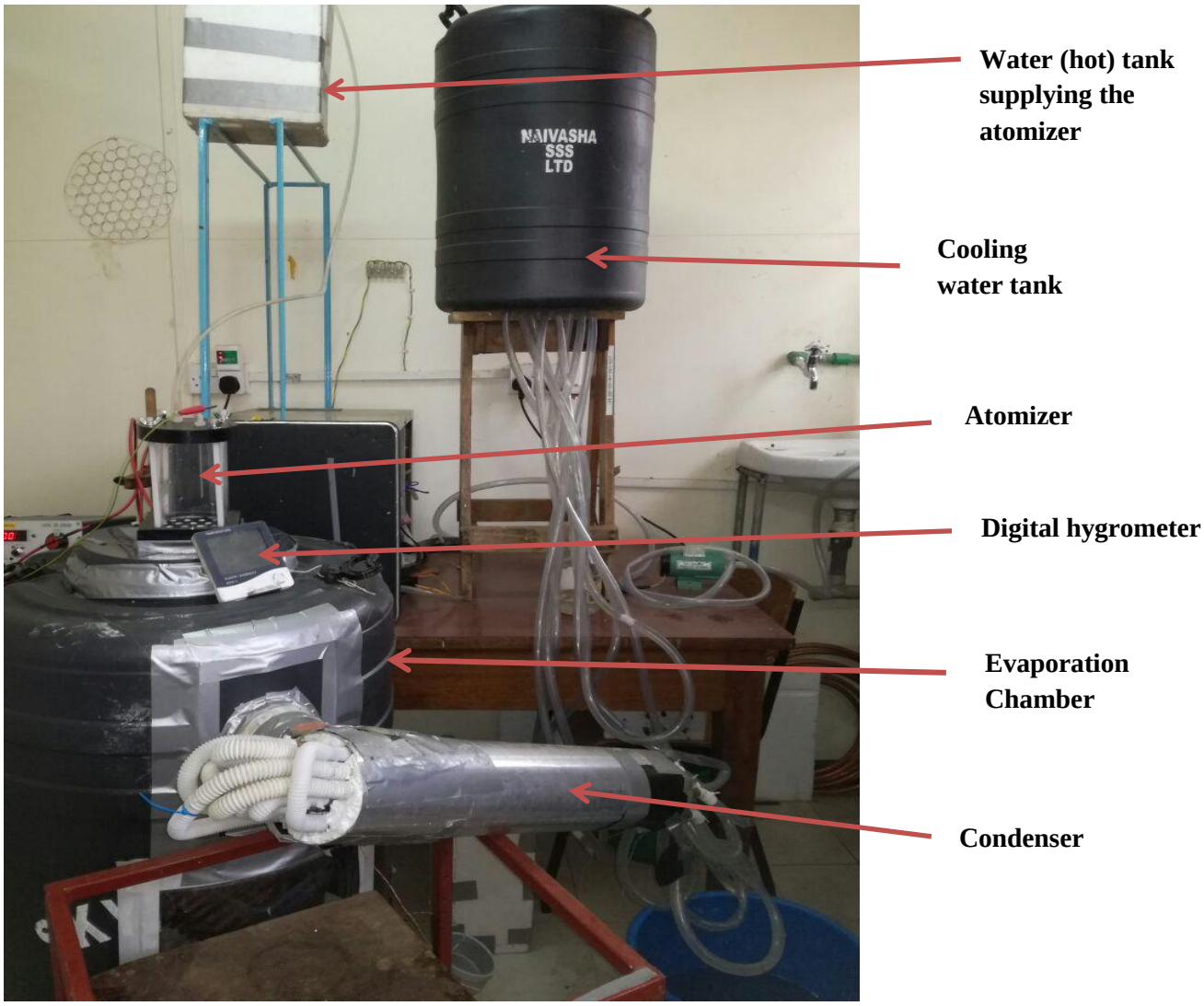

Figure 22. The experimental set-up

Hot water was supplied to the atomizer fixed at the top of the evaporation chamber. The atomizer breaks up the water into small droplets which provide a large surface area for evaporation. The chamber is fitted with a hygrometer and digital temperature probe to monitor the temperature and the relative humidity inside the evaporation chamber.

The moist air inside the evaporation chamber is then pushed out by the suction fan and directed into the condenser. The condenser receives cooling water from the cooling water tank. The condensed water is then collected and the volume measured.

The test run of the condenser showed that the design velocity of 4.0 m s^{-1} would not be achieved by the experimental prototype because of the large amounts of cooling water needed. To achieve this, a pumping system would be required. The velocity that was achieved was 0.215 m s^{-1}; this velocity was due to gravitational flow and it represented a Re value of 2300 implying the transitional flow regime. The measurements that were taken during the experiments were: the relative humidity, temperature of the moist air exiting the chamber into the condenser, amount of water put into the system and the amount of brine collected. All these were taken over a specified period of time. The highest relative humidity that was achieved on average from the experiments was 73%. The cooling water was cooled using ice (from a refrigerator). However, in practice, the cooling water will be cooled to the wet bulb temperature of 15 – 18^{o}C.

The following experiments were carried out and the results are tabulated in Table 20:

Table 2. Experiment: Determination of Evaporation Rate

Time (Minutes)	**Relative Humidity (moist air) (RH) %**	**Evaporation Chamber Temperature (^{o}C)**
0	46	45
5	56	34
10	65	33
15	74	33
20	78	33
25	81	33
30	85	33
35	85	33
40	87	33
45	81	33
50	81	33
55	81	33
60	89	33
Average	72	35

The amount of saline water put in to the system for one hour was 3.315 litres and the amount of brine collected after an hour was 2.218 litres. Using mass balance, the amount or water evaporated in an hour was (3.315 litres - 2.218 litres) 1.097 litres. Therefore the was evaporation rate was 1.097 l hr^{-1} implying 0.018 l min^{-1}

Table 3. Experiment Run 1. Determination of Mass of Condensate

Time (minutes)	**Relative Humidity (moist air) (RH) %**	**Inlet Temperature of Cooling Water (T_{c1}), (^oC)**	**Temperature of the moist air into the condenser (^oC)**
0	40	3	39
5	72	3	37
10	75	3	35
15	80	4	33
20	84	5	32
25	89	7	32
30	90	7	31
Average	73	5	34

The amount of saline water put in to the system for 30 mins was 3180 ml. The amount of condensate collected in 30 mins was 215ml.Therefore the amount of water evaporated in 30 mins was given by:.

Evaporation rate * time = 0.018 l min^{-1} *30 mins

= 0.540 litres

The Evaporation Efficiency was determined as:

$$\frac{Volume\ of\ the\ Evaporate}{Total\ Volume\ put\ into\ the\ system} * 100 = \frac{0.540\ l}{3.180\ l} * 100 = 17\%$$

Where:

Mass flow rate of condensate in kg $\mathbf{s^{-1}}$ was$1.3 * 10^{-4}$

Mass flow rate of water vapor at kg $\mathbf{s^{-1}}$ was $3.0 * 10^{-4}$

Outlet temperature of cooling water (T_{c2}) was 8^oC

Temperature difference between T_{c1} and T_{c2}, ΔT was 3^0C

The Recovery Ratio was determined as:

$$\frac{Volume\ of\ Condensate}{Total\ Volume\ put\ into\ the\ System} = \frac{215\ ml}{3180ml} * 100 = 6\%$$

The recovery ratio is also given by: evaporation efficiency * condensation efficiency. Therefore;

$$\text{condensation efficiency} = \frac{\text{recovery ratio}}{\text{evaporation efficiency}} * 100 = \frac{6}{17} * 100 = 35\%$$

However, during this experiment, the condenser was found to have leakages which caused some of the moist air from the evaporation chamber to escape before condensation. These leakages were sealed and the experiment was conducted again.

Table 4. Experiment Run 2. Determination of Mass of Condensate

Time (minutes)	**Relative Humidity (moist air) (RH) %**	**Inlet Temperature of Cooling Water (T_{c1}), (^oC)**	**Temperature of the moist air into the condenser (^oC)**
0	42	14	49
5	63	16	43
10	70	17	41
15	79	18	42
20	86	18	39
25	89	19	38
30	90	20	38
Average	73	19	40

The amount of saline water put in to the system for 30 mins was 3180 ml. The amount of condensate collected in 30 mins was 225 ml. Therefore, the amount of water evaporated in 30 mins was given by:.

Evaporation rate * time = 0.018 l min^{-1} *30 mins

= 0.540 litres

The evaporation efficiency was determined as:

$$\frac{Volume\ of\ the\ Evaporate}{Total\ Volume\ put\ into\ the\ system} * 100 = \frac{0.540\ l}{3.180\ l} *100 = 17\%$$

Where:

Mass flow rate of condensate in kg $\mathbf{s^{-1}}$ was $1.3 * 10^{-4}$

Mass flow rate of water vapor at kg $\mathbf{s^{-1}}$ was $3.0 * 10^{-4}$

Outlet temperature of cooling water (T_{c2}) was 21 ^{o}C

Temperature difference between T_{c1} and T_{c2}, ΔT was 2^{0}C

The Recovery Ratio was determined as:

$$\frac{Volume\ of\ Condensate}{Total\ Volume\ put\ into\ the\ System} = \frac{225\ ml}{3180 ml} * 100 = 7\ \%$$

The recovery ratio is also given by: evaporation efficiency * condensation efficiency. Therefore;

$$\text{condensation efficiency} = \frac{\text{recovery ratio}}{\text{evaporation efficiency}} * 100 = \frac{7}{17} * 100 = 41\%$$

Table 5. Experiment Run 3. Determination of Mass of Condensation

Time (minutes)	**Relative Humidity (moist air) (RH) %**	**Inlet Temperature of Cooling Water (T_{c1}), (^{o}C)**	**Temperature of the moist air into the condenser (^{o}C)**
0	42	4	45
5	52	5	34
10	58	5	33
15	68	7	33
20	75	8	33
25	82	9	33
30	86	10	33
Average	69	7	35

The amount of saline water put in to the system for 30 mins was 3180 ml. The amount of condensate collected in 30 mins was 285 ml. Therefore, the amount of water evaporated in 30 mins was given by:.

Evaporation rate * time = 0.018 l min^{-1} *30 mins

= 0.540 litres

The Evaporation Efficiency was determined as:

$$\frac{Volume\ of\ the\ Evaporate}{Total\ Volume\ put\ into\ the\ system} * 100 = \frac{0.540\ l}{3.180\ l} * 100 = 17\%$$

Where:

Mass flow rate of condensate in kg $\mathbf{s^{-1}}$: $2.0 * 10^{-4}$

Mass flow rate of water vapor mixture at kg $\mathbf{s^{-1}}$: $3.0 * 10^{-4}$

Outlet temperature of cooling water (T_{c2}): $10^{o}C$

Temperature difference between T_{c1} and T_{c2}, ΔT: $3^{0}C$

The Recovery Ratio was determined as:

$$\frac{Volume\ of\ Condensate}{Total\ Volume\ put\ into\ the\ System} = \frac{285\ ml}{3180ml} * 100 = 9\%$$

The recovery ratio is also given by: evaporation efficiency * condensation efficiency. Therefore;

$$\text{condensation efficiency} = \frac{\text{recovery ratio}}{\text{evaporation efficiency}} * 100 = \frac{9}{17} * 100 = 54\%$$

4.4 Simulation of Condenser Performance

This section outlines the results of the modelling done with Matlab-Simulink program. The simulation was aimed at predicting the performance of the condenser when subjected to different conditions.

4.4.1 Mass of Condensate

The simulation was done for different values of relative humidity (RH) of the moist air that is; 70%, 50% and 40% and cooling water temperatures; 5°C, 10°C, 15°C and 20°C. The selected relative humidity values were based on the experiments that were ran. The simulation was based on a velocity of cooling water of 0.215 m s^{-1} and a temperature of the moist air from the evaporation chamber of 35°C (from experiments).

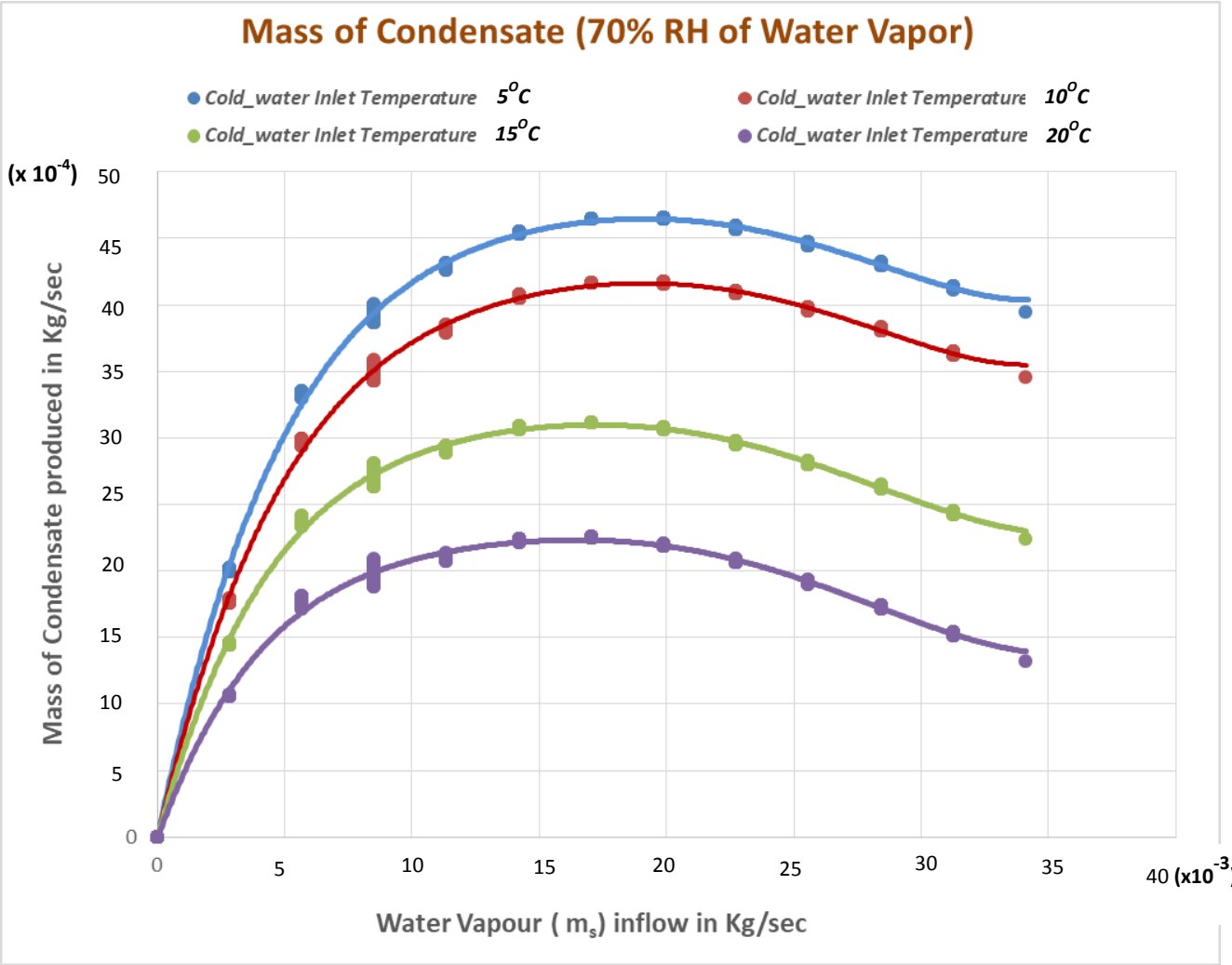

Figure 23a. Mass flow rate of condensate (kg s^{-1}) at 70% relative humidity of moist air

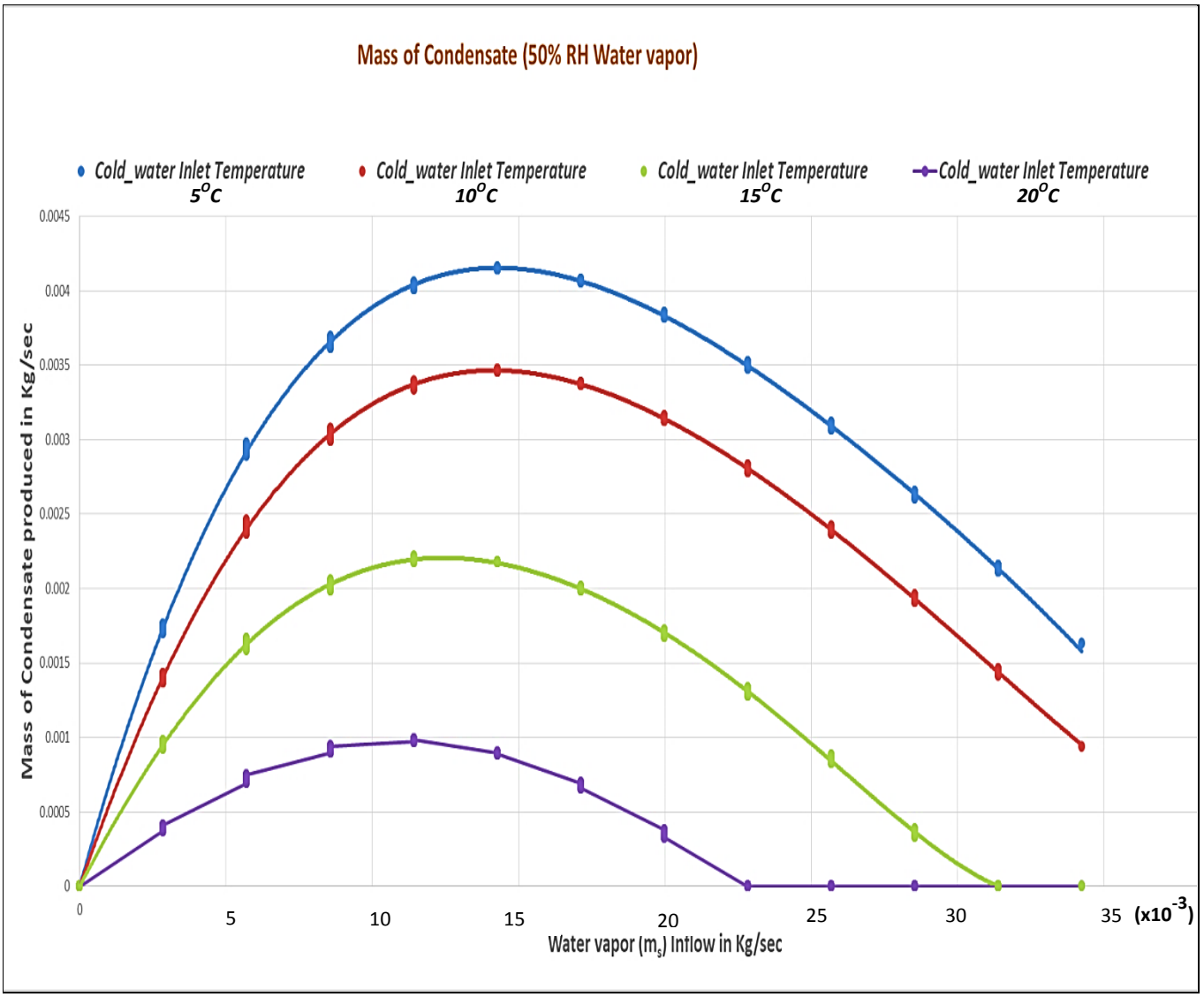

Figure 23b. . Mass flow rate of condensate (kg s^{-1}) at 50% relative humidity of moist air

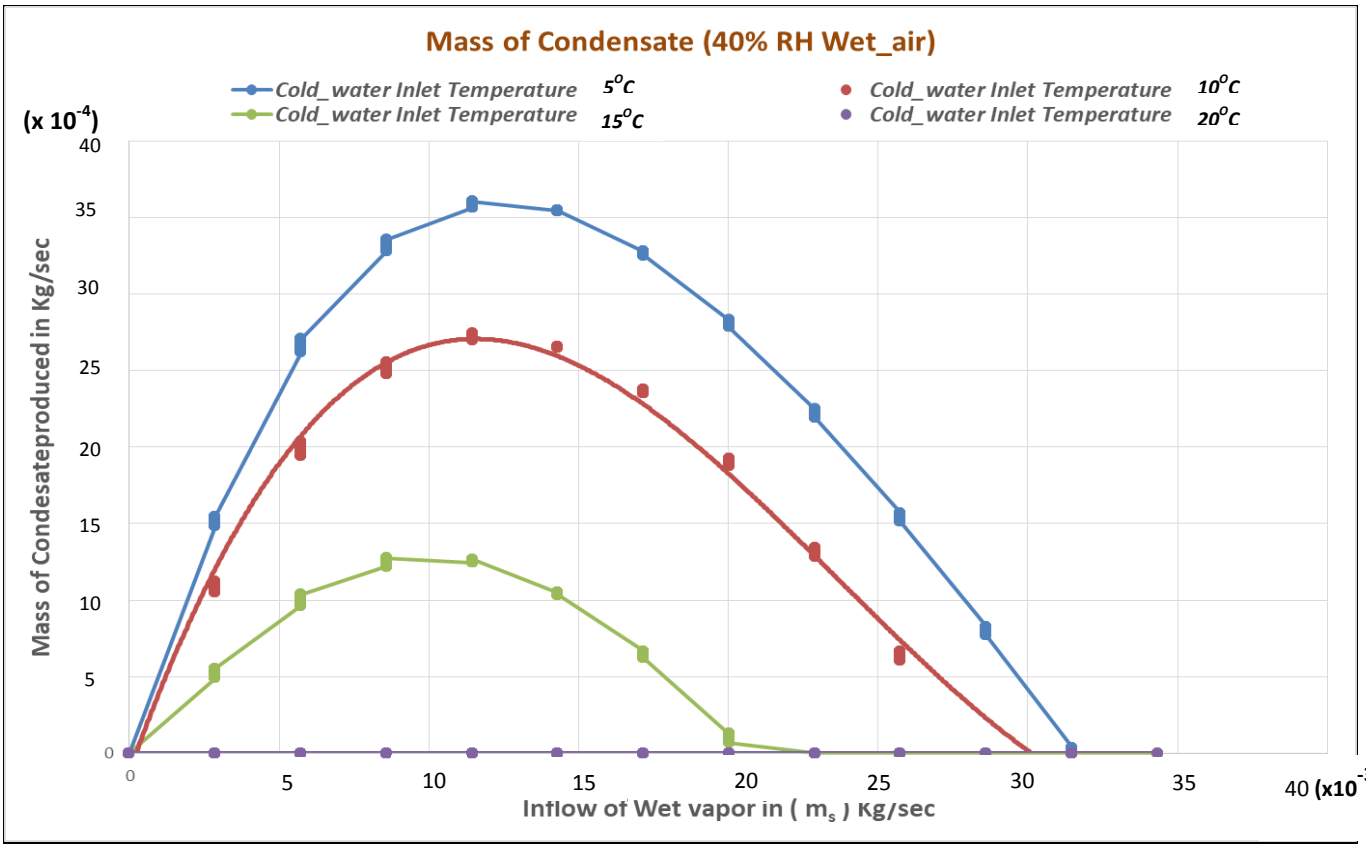

Figure 23c. Mass flow rate of condensate (kg s^{-1}) at 40% relative humidity of moist air

.

Figures 23a, 23b and 23c show that as the mass flow rate of the water vapor (m_s) increases, the mass of the condensate also increases. However, the increase is up to a certain point (peak). The mass of the condensate then plateaus before it starts to decline. The peaks of the graphs indicate the optimal mass flow rate of water vapor, m_s for the condenser. Beyond this plateau region, the mass flow rate of the incoming water vapor is very high. As a result, the residence time in the condenser is short and therefore most of the vapor escapes without condensing. This decreases the mass of condensate produced.

Figures 23a, 23b and 23c also show that as the temperature of the cooling water increases from 5°C to 20°C, the amount of condensate reduces. This is because the temperature difference between the water vapor (35°C) and the cooling water decreases. The higher the temperature differences between the two fluid streams, the greater the rate of heat transfer. Furthermore, figures 23a, 23b and 23c also indicate that higher values of RH give better condensation. This is because higher values RH imply that a specific volume of air contains more vapour.

Figures 24a and 24b show the efficiency of condensation at different RH values. At the higher RH value of 70%, the highest efficiency was 78% using cooling water at a temperature of 5°C. This efficiency decreases with increase in cooling water temperature and reduced relative humidity. This is evident in Figure 23b where the efficiency is 16% for a RH value of 50% and cooling water temperature of 20°C.

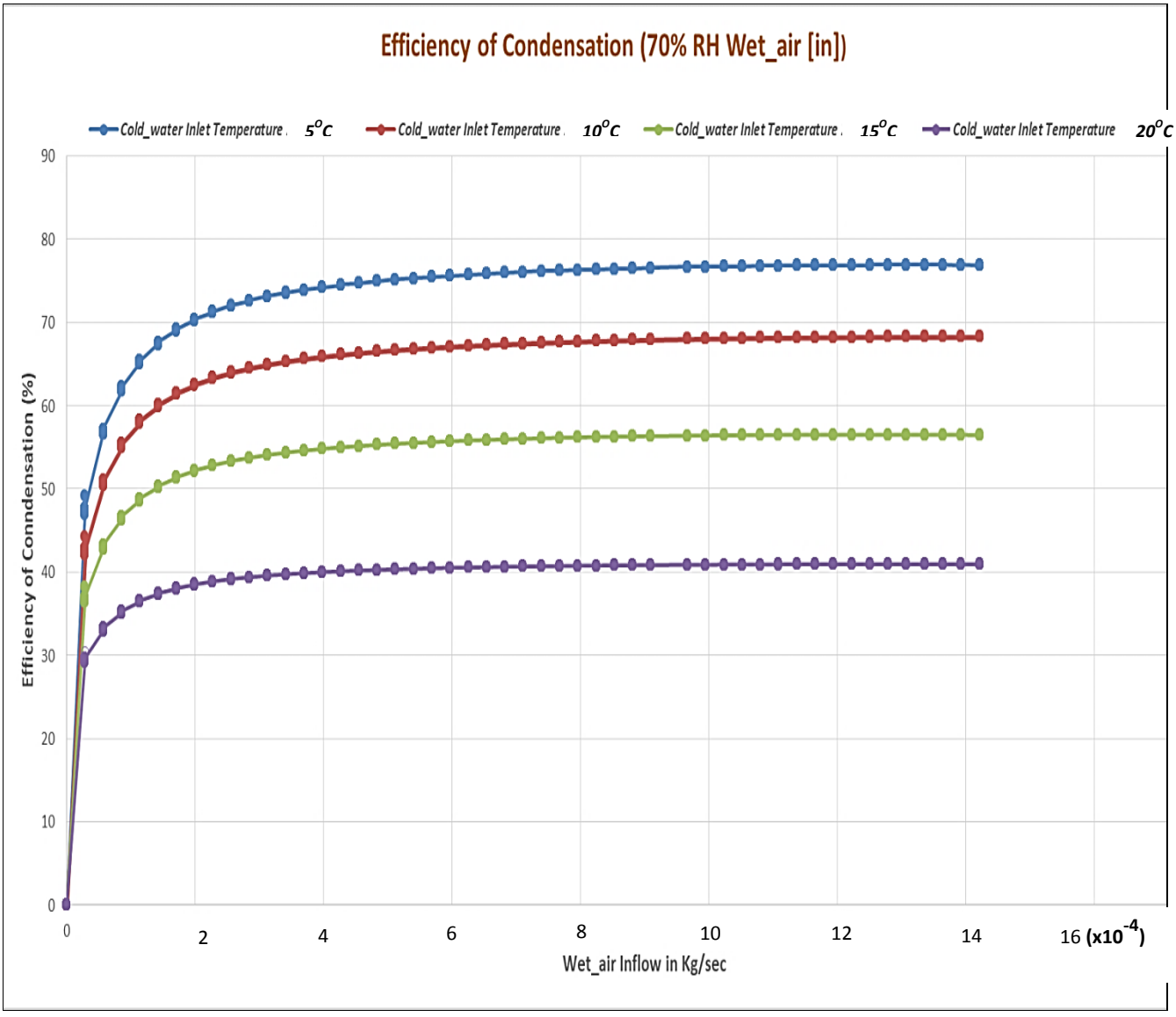

Figure 24a. Efficiency of Condensation at 40% relative humidity of moist air

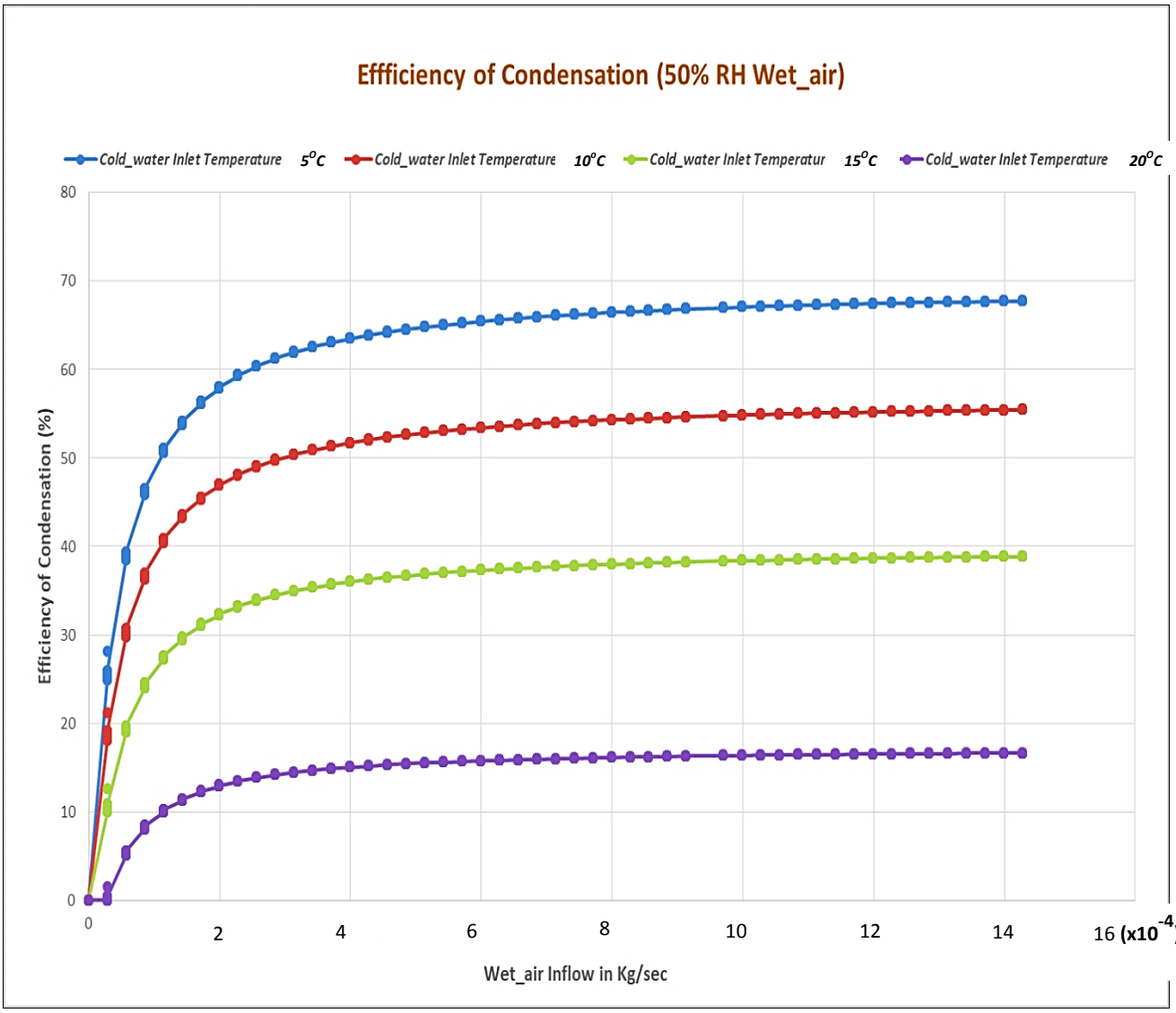

Figure 24b. Efficiency of condensation at 50% relative humidity of moist air

4.4.2 The Outlet Temperature of the Cooling water (T_{c2})

Figures 25a and 25b give the outlet temperature of the cooling water (T_{c2}). Depending on the inlet temperature of the cooling water (T_{c1}), the graphs are used to determine the temperature difference, ΔT , between T_{c2} and $T_{c1.}$ From the graphs, the average ΔT is 2 ^{o}C.

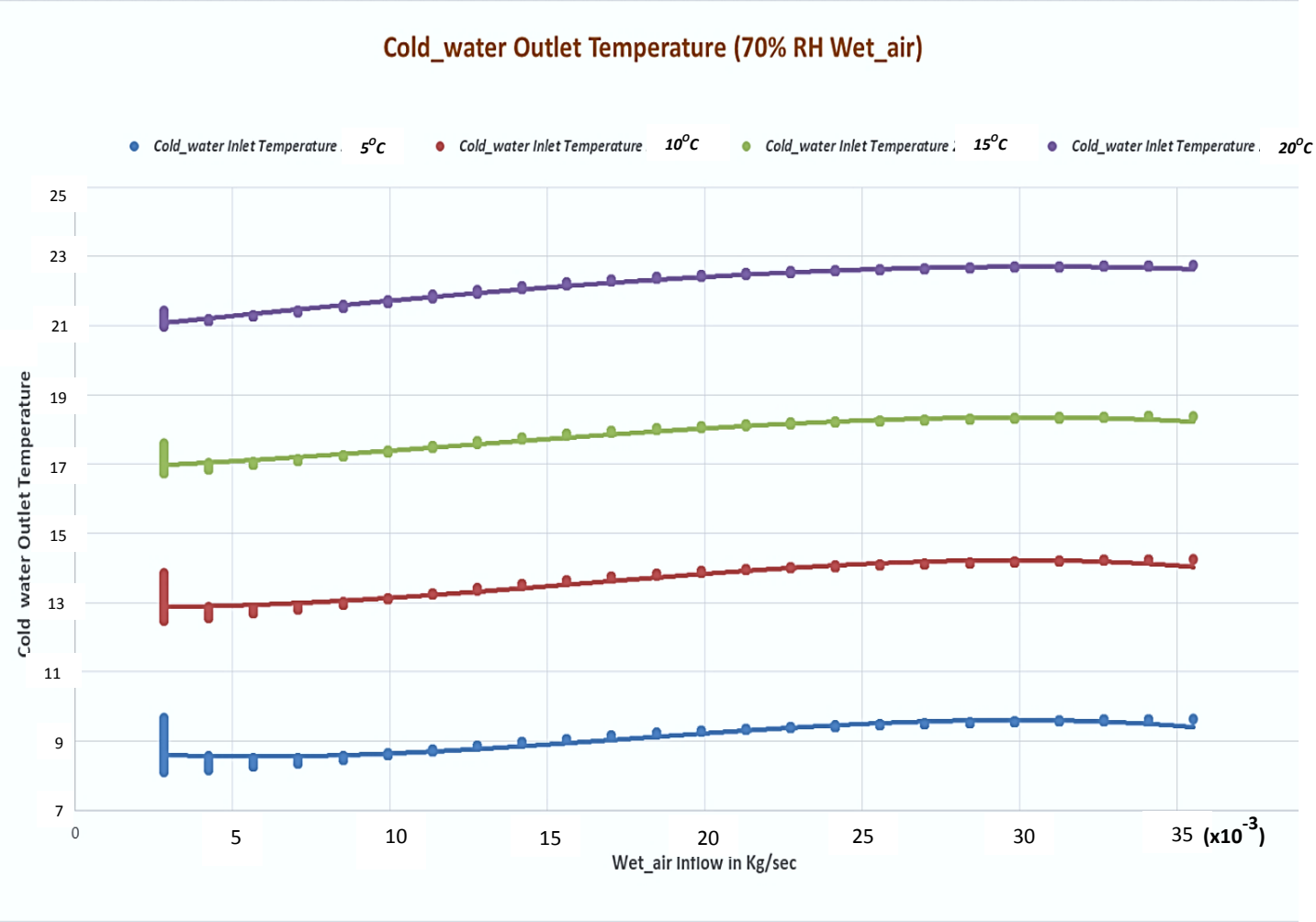

Figure 25a. Outlet temperature of the cooling water (T_{c2}) at 70 % relative humidity of moist air

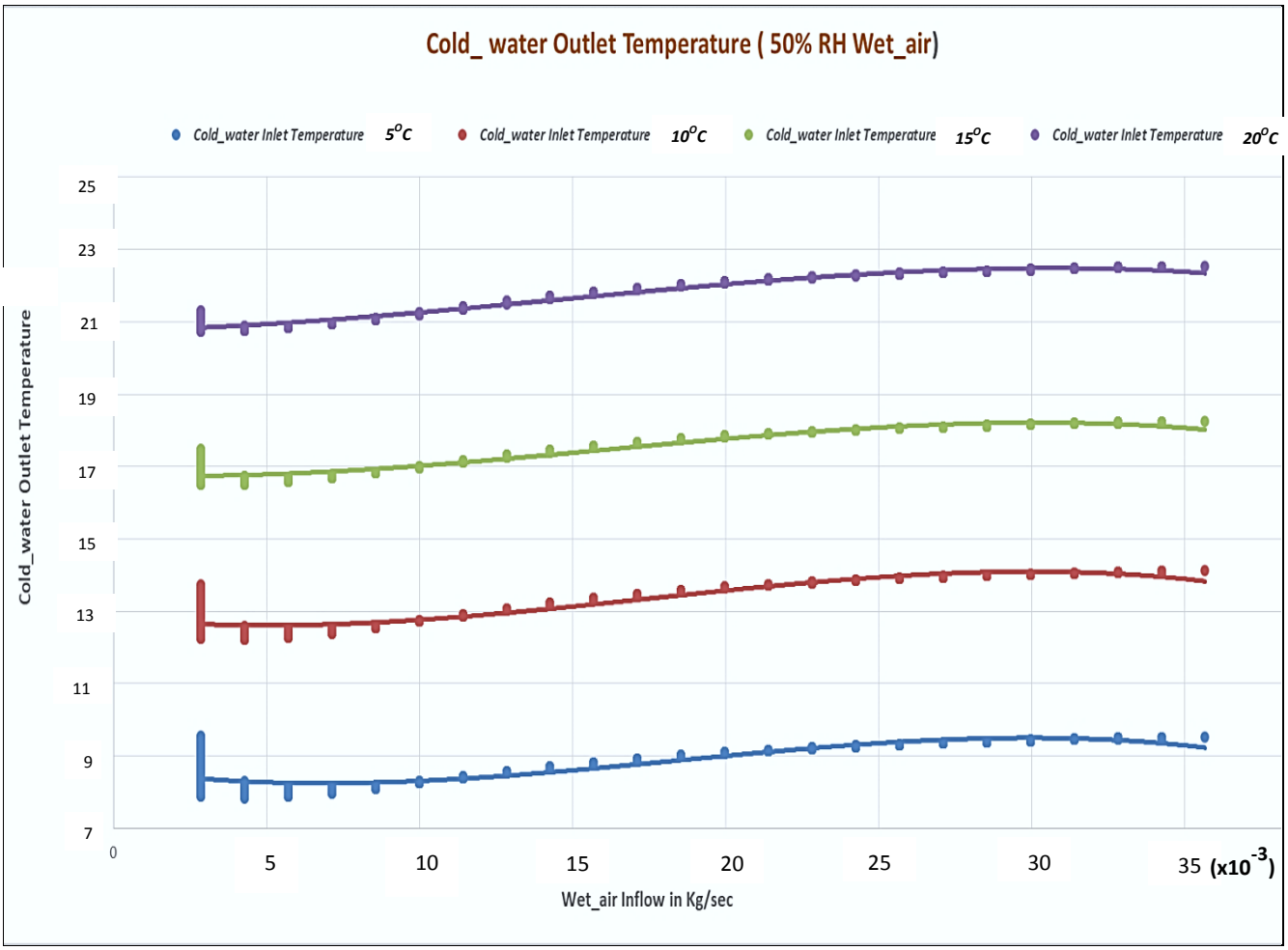

Figure 25b. Outlet Temperature of the Cooling water (T_{c2}) at 50 % relative humidity of moist air

4.5 Validation Analysis

This section shows the comparison between the experimental values (*Section 4.3*) and the simulated values (*Section 4.4*).

4.5.1 Mass of the Condensate

From experiment run 1 (*Section 4.3*), the value of the mass flow rate of condensate was $1.3*10^{-4}$ kg s^{-1}. The value of the mass flow rate of condensate from the simulation at 70% RH, T_{c1} at $5^{o}C$ (278K) and $3.0*10^{-4}$ kg s^{-1} flow of vapor was $2.4*10^{-4}$ kg s^{-1}. This shows a difference of $1.1*10^{-4}$ kg s^{-1}. The simulated value differs from the experimental value by 80%, clearly, a wide difference. This difference was attributed to the condenser leakage that caused some of the moist air from the evaporation chamber to escape. This leakage was sealed and more experiments were conducted.

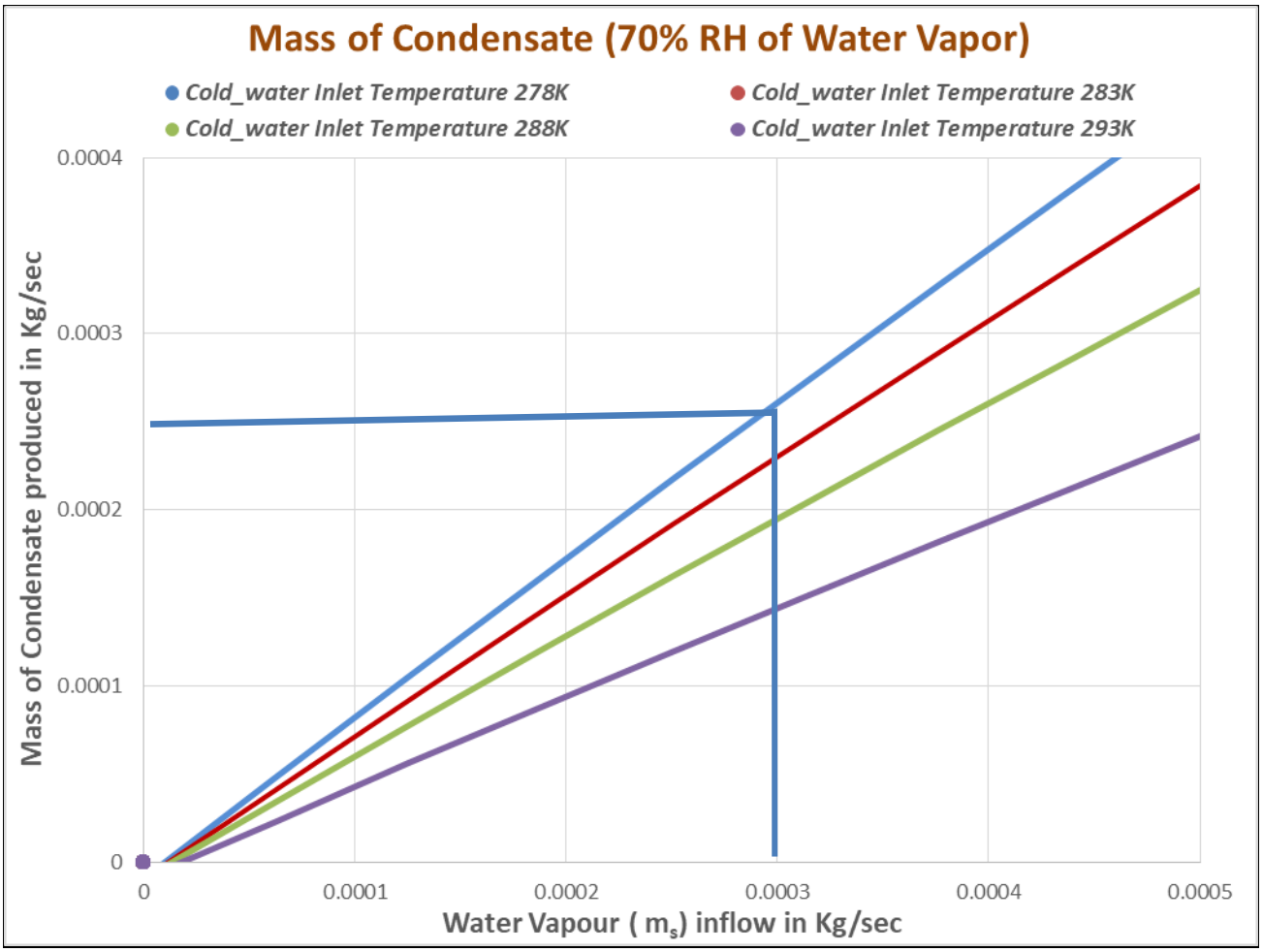

Figure 26a. Mass flow rate of the condensate: Simulated results vs. experimental results (Experiment Run1)

From experiment run 2 (*Section 4.3*), the value of the mass flow rate of condensate was$1.3*10^{-4}$ kg s^{-1}. The value of the mass flow rate of condensate from the simulation at 70% RH, T_{c1} at 20^{o}C (293K) and $3.0*10^{-4}$ kg s^{-1} flow of vapor was $1.5 *10^{-4}$ kg s^{-1}. This shows a difference of 0.00002 kg s^{-1}. The simulated value differs from the experimental value by 16 %.

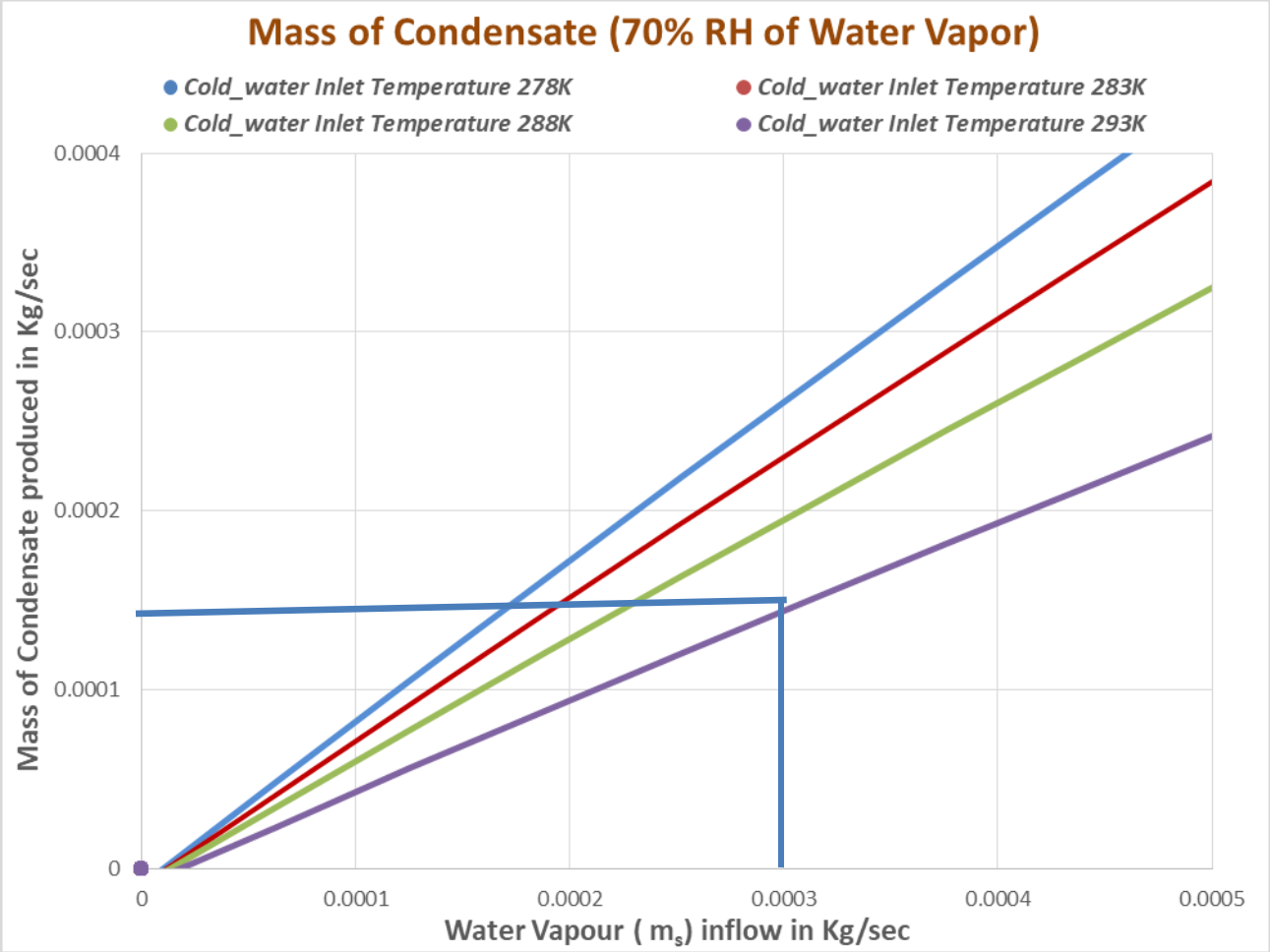

Figure 26b. Mass flow rate of condensate: Simulated results vs. experimental results (Experiment Run 2)

From experiment run 3 (*Section 4.3*), the value of the mass flow rate of condensate was $2.0*10^{-4}$ kg s^{-1} at 7^{o}C. The value of the mass flow rate of condensate from the simulation at 70% RH, T_{c1} at 5^{o}C (278K) and $3.0*10^{-4}$ kg s^{-1} flow of vapor was $2.4 *10^{-4}$ kg s^{-1}. Also, the value of the mass flow rate of condensate 70% RH, T_{c1} at 10 ^{o}C (283K) and $3.0*10^{-4}$ kg s^{-1} flow of vapor is $2.3 *10^{-4}$ kg s^{-1}. Interpolation was done between the two points to get the value at 7^{o}C. The mass

flow rate of the condensate at 70% RH, T_{c1} at 7°C (280K) and $3.0*10^{-4}$ kg s^{-1} flow was $2.3*10^{-4}$ kg s^{-1}. This shows a difference of $3.0*10^{-5}$ kg s^{-1}. The simulated value differs from the experimental value by 15 %. The variance between the simulated values vs. the experimental values in Experiment run 3 shows a small difference from Experiment run 2.

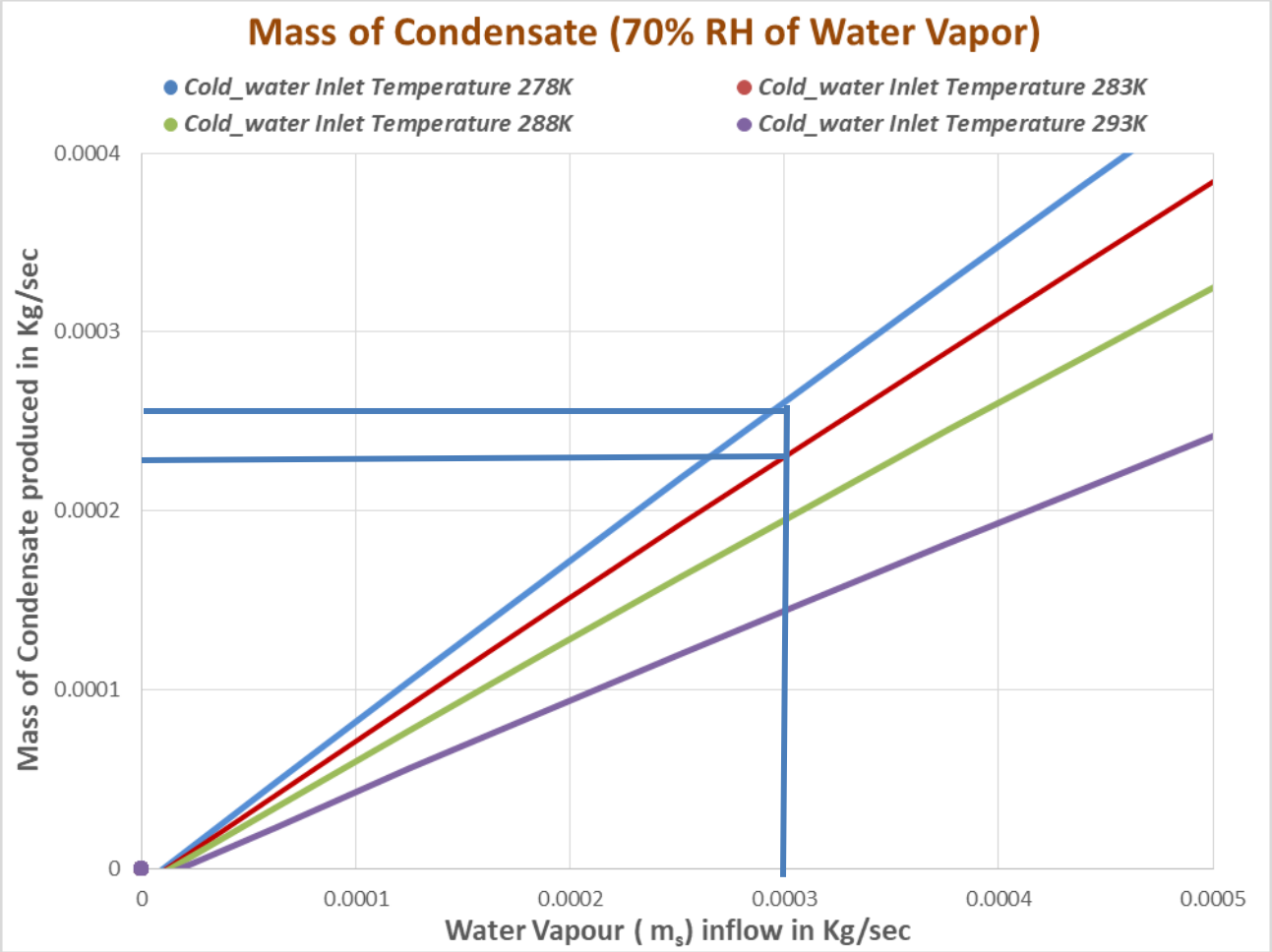

Figure 26c. Mass flow rate of condensate: Simulated results vs. experimental results (Experiment Run 3)

4.5.2 The Outlet Temperature of Cooling Water (T_{c2})

Experiments run 1, 2 and 3 (*Section 4.3*); the outlet temperature of cooling water (T_{c2}) was 8^{o}C, 21^{o}C and 10^{o}C respectively. The average inlet temperature of cooling water (T_{c1}) for experiment run 1, 2 and 3 was 5^{o}C, 19^{o}C and 7^{o}C respectively. Therefore, the ΔT for experiment run 1, 2 and 3 was 3^{o}C, 2^{o}C and 3^{o}C respectively.

From the simulation at 70% RH, the graph at T_{c1} of 20^{o}C show an average ΔT of 2^{o}C and the graph at T_{c1} of 5^{o}C shows an average ΔT of 3^{o}C (*see Figure 25a*). The results from experiment run 2 (70% RH and T_{c1} of 19^{0}C) have ΔT of 2^{o}C and the simulated results (70% RH and T_{c1} of 20^{0}C) show ΔT of 3^{o}C. For Experiment run 1 and 3, the ΔT is 3^{o}C and 3^{o}C respectively. Both of these experiments were performed at 70% RH and at a temperature of ~5^{o}C. The simulation graphs give ΔT of 3 ^{o}C. The simulated and experimental results show a small difference.

Chapter Five

Conclusions and Recommendations

The scope of this work was to design and fabricate a condensation system to provide the optimum water vapor condensation parameters for the innovated Thermal Desalination System (*Figure 7*). This included selecting the best heat exchanger system to suit the desalination system; modelling the chosen heat exchanger; fabrication of the heat exchanger; simulation analysis and carrying out experiments to validate the simulation results.

The shell and tube heat exchanger (STHE) was chosen. This type of exchanger is made up of an array of tubes with each of the tubes at a specified distance from the other. Cooling water runs through the tubes. The tubes are then covered with a shell. The moist air travels through the shell where it gets into contact with tubes and finally condenses on the surface of the tubes. The STHE was modelled using the iterative Kern Model (Kern, 1950). The model gave the design parameters. Using the design parameters given by the model, the condenser was fabricated. The tubes and shell were of copper and aluminium material respectively. The condenser was then attached to the evaporation chamber of the desalination system and experiments were run. Simulation was then done using the Matlab-Simulink software to predict the performance of the condenser. The simulation conditions were dictated by the experiments conducted. The simulated and experimental results were then compared for validation analysis.

The following was noted:

a) Higher relative humidities favor condensation. At a relative humidity of 40% and condenser cooling water inlet temperature of $20^{o}C$ the rate of condensation is almost negligible
b) The larger the temperature difference, ΔT, between the hot fluid and cold fluid streams in the condenser the higher the rate of condensation
c) The temperature rise of the cooling water between the inlet and outlet of the condenser was on average $2^{o}C$
d) The simulation results showed, on average, 15% difference from the experimental results. This difference was reasonable especially considering that the measuring instruments were not suitable and the model can be used to make predictions on the performance of the condenser.

e) Matlab/Simulink program with a Thermodynamic (Thermolib) library add-on can be used to model the operation of heat exchanger under varying conditions and the model results give the performance of the heat exchanger.

For further research the following is recommended:

a) Cooling from the condenser should be recirculated. Results from the experiments and simulation indicate that the average temperature difference between the inlet and outlet cooling water temperature (ΔT) is 2^oC. This ΔT is small. Recirculation will save on the amount of water and energy used. More energy will be spent initially to cool the water to the wet-bulb temperature. After this, less energy will be required for cooling since the temperature rise is, on average, 2^oC.

b) The evaporation system should be designed in such a way as to produce larger amounts of water vapor. Using the 'mass flow rate of condensate' graphs (Figures 23a, 23b & 23c), the results from the experiments show that the mass flow rate of water vapor is quite low. Experiments at 70% RH (*Section 4.3*) indicate that the mass flow rate of the water vapor is $3.0*10^{-4}$ kg s^{-1}. This value lies in the lower region of the 'mass flow rate of condensate' graphs (Figure 23a) of 70% RH. The desired result is that this value climbs up on the mass of condensation graphs. This implies that incoming humid air from the evaporation chamber gives an optimal water vapor mass flow rate of $1.5*10^{-2}$ to $2.0*10^{-2}$ kg s^{-1} depending on the conditions.

c) The condenser should operate at higher relative humidity. A relative humidity of 40% and below 40% gives negligible condensation rate.

References

Adelaja, A., Ojolo, S., and Sobamowo, G., (2011). *Computer Aided Analysis of Thermal and Mechanical Design of Shell and Tube Heat Exchangers*. Journal of Advanced Materials Research Vol 367 (2012), Pages 731-737.

Bell, K.J., (1963). *Final report of the cooperative research program on shell-and-tube heat Exchangers.* University of Delaware Eng. Exp. Stat. Bull. 5.

Coulson, J.M. and Richardson, J. F., (1999). *Chemical Engineering; Fluid flow, Heat Transfer and Mass Transfer*. Oxford, GB, Vol.1 6th Edition

Dirkse, M.H., Loon, W.K.P., and Bot, G.P.A., (2006). *Computational Fluid Dynamics Model for Designing Heat Exchangers based on Natural Convection.* Elsevier Journal of Bio systems Engineering Vol.94, Issue 3 (2006), Pages 443-452

Food and Agricultural Organization (FAO) of the United Nations, (2015). *Sustainable Land Management.* Retrieved January 12, 2017 from http://www.fao.org/nr/land/sustainable-land-management/farmer-field-school/agro-pastoral-ffs-project-home/ffs/en/

Hasu, B.S., and Rao, G.V.S., (2017). *Design and Analysis of a Heat Exchanger with Helical Baffles by using CFD.* International Journal of Engineering Trends and Technology Volume 48, No.7 (June 2017), Pages 350-353. ISSN: 2231-5381.

Incropera, F. P., DeWitt, D. P., Bergman, T. L., and Lavine, A. S., (2007). *Fundamentals of Heat and Mass Transfer*. Wiley, USA, 6th edition.

Jingwe, H.C., Wang, D., Gao, X., and Gao, C. (2011). *Desalination* 258, 5-11

Joydeep, B., and Ghoshal, A.K., (2007). *Performance analysis of finned tube and unbaffled shell-and-tube heat exchangers.* Elsevier International Journal of Thermal Sciences Volume 46, Issue 12 (2007), Pages 1311-1317.

Karno, A., Ajib, S., (2005). *Effect of tube pitch on heat transfer in shell-and-tube heat Exchangers - new simulation software*. Journal of Heat Mass Transfer Volume 42 (2006), Pages 263-270.

Kakaç, S., Liu, H., and Pramaunjaroenkij, A., (2012). *Heat Exchanger: Selection, Rating and Thermal Design.* CRC Press, 6000 Broken Sound Parkway NW, Suite 300 Boca Raton, FL 33487-2742, Third Edition (2012).

Kern, D.Q., (1950). *Process Heat Transfer*. McGraw-Hill, New York. Inc., (1983), pp. 226

Kumaresan, G., Rantosh, R., Duraisamy, P., Venkatesan, R., and Kumar, N.S, (2017). *Numerical Analysis of Baffle Cut on Shell Side Heat Exchanger Performance with Inclined Baffles.* Journal of Heat Transfer Engineering (2017), Pages 1-10.

Mukherjee, R., (1992). *Use Double-Segmental Baffles in Shell-and-Tube Heat Exchangers*. Chem. Eng. Progress, 88 (11), pp. 47–52.

Mishra, R.K., and Dubey, S. C (2015). *Fresh water availability and its global challenge*. International Journal of Engineering Science Invention Research & Development Vol 2, No. 6, page 351.

UN, United Nations; OHCHR, Office of the High Commissioner for Human Rights; UN-HABITAT, United Nations Human Settlements Programme and WHO, World Health Organization (2010). *Right to Water*, Fact Sheet No. 35.

Qiao He and Wennan Zhang, (2001*). A study on latent heat storage exchangers with the high-temperature phase-change material.* International Journal of Energy Research Volume 25, Issue 4 (2001), pages 331–341

Rajput, R.K., (2008). *Textbook of Heat and Mass Transfer SI Units.* S. Chand, New Delhi, India.

Reppich, M., Zagermann, S., (1995*). New design method for segmentally baffled heat Exchangers*. International Journal of Computer and Chemical Engineering Vol.19 (Suppl.) S137- S142

Saunders, E.A.D., (1988). *Heat Exchangers*. John Wiley & Sons, New York, 1988.

Shah, R.K., (1981). *The Transient response of Heat Exchangers*. Heat Exchangers Thermal Hydraulic Fundamentals and Design, Hemispheres Publications, New York, 1981

Taylor, R.G., Mileham, L., Tindimugaya, C., Majugu, A., Nakileza, R., Muwanga, A., (2006). *Recent deglaciation in the Rwenzori Mountains of East Africa due to rising air Temperatures*. Geophysical Research Letters Vol. 33, L10402.

Thundil, R., Raj, K., and Ganne, S., (2012*). Shell side numerical analysis of a shell and tube heat exchanger considering the effects of baffle inclination angle on fluid flow*. International Journal of Thermal Science Vol. 16, No. 4 (2012), Pages 1165–1174.

Tinker, T., (1951). *Shell-side characteristic of shell-and-tube heat exchangers, Parts II, III, And I.* Proceedings of General Discussion on Heat Transfer, Institute of Mechanical Engineers and American Society of Mechanical Engineers, London, New York, 1951, p. 89.

WHO, World Health Organization, 2012. *Health and Water Fact Sheet*. Retrieved February 8, 2017, from http://www.afro.who.int/en/health-topics/topics/4415-water.html

WHO, World Health Organization; UNICEF, United Nations International Children's Emergency Fund and WWI, World Watch Institute, (2006). *Meeting the MDG's Drinking Water and Sanitation Target*. Geneva.